Computational Studies on the Robustness of the H^∞ Feedback Control in a 2-D Structural Acoustic Model with Periodic Excitation *

H. T. Banks[†] **M. A. Demetriou**[†] **R. C. Smith**[‡]

April 24, 1995

Abstract

An extensive study on the robustness of the H^∞ compensator for the 2-D structural acoustic model is undertaken. The effects of frequency uncertainties in an exogenous periodic signal are studied for both the case where it is contained in the controller formulation and the case where it is excluded. Time delays are inserted in the input and/or output signals and their effect on the controller performance is recorded. Additionally, the effects of phase shifts and discrete time approximations are studies along with those of time delays. A comparison between the standard LQG/Kalman filter and the H^∞-Minmax compensator reveals no significant differences in the overall controller performance. Modifications in the controller structure are studied to see whether loss of information (the tracking signal) that must be calculated apriori would result in performance degradation. This study provides a valuable insight on the computational and implementational issues that arise when dealing with the control of large and complex systems that are governed by partial differential equations.

1 Introduction

The H^∞/MinMax robust control methodology is applied most often to systems in a manner so as to guarantee a robustness margin in the presence of uncertainties in the model (modelling errors) and uncertainties in the performance output (measurement errors). The resulting H^∞-based compensator guarantees (under certain system assumptions including detectability, stabilizability, invariant zeros condition) that the H^∞-norm of the closed loop transfer function from the disturbance to the performance output signal is less than a certain prescribed bound γ. If a known exogenous input (a persistent disturbance that is assumed to be known at all times), is applied to the system, a modification to the controller/compensator theory can be made in order to account for the presence of such a signal. An additional tracking variable is then coupled to the familiar H^∞ control law.

*Research supported in part (H.T.B. and M.A.D.) by the Air Force Office of Scientific Research under grant AFOSR F49620-93-1-0198, and in part (M.A.D. and R.C.S.) by NASA under grant NAG-1-1600. Research also supported in part by NASA under contracts NAS1-18605 and NAS1-19480 to ICASE while H.T.B. and R.C.S. were visiting scientists at ICASE, NASA Langley Research Center.

†Center for Research in Scientific Computation, North Carolina State University, Raleigh, NC 27695-8205

‡Department of Mathematics, Iowa State University, Ames, IA 50011

In practice, implementation of such a modified control law (a "tracking H^∞ controller") would require the complete knowledge of the exogenous signal from the present time to the future. This is necessary due to the causal nature of the original system; the tracking signal must first be generated (integrated) backward in time and then used in the control law. This often makes implementation of the tracking H^∞ control law rather difficult if not impossible. In the event that such an exogenous input is known to be periodic with a known period, then one can take advantage of this periodicity in that the tracking signal may be integrated backward through only one period at a time, thus rendering possible a practical implementation of the tracking H^∞ control law (see [7] for a general discussion).

This report summarizes our computational findings for the H^∞/MinMax control of a structural acoustic model in which piezoceramic patches are used to excite a closed structure for control of transverse vibrations and a coupled interior cavity acoustic pressure field. An exterior noise field (exogenous input) excites the structure thus producing vibrations which in turn produce interior cavity noise. Following [3], [4], an extensive study was undertaken to study the effects of an exogenous input (the exterior noise field which in our computational studies was produced by a simulated force to the structure) on the performance of the H^∞ compensator. Difficulties arise when delays in the input or output signal enter in the controller, or when uncertainties in the exogenous signal are present. Time delays enter the control system through the input signal where they result from digital to analog conversion. Another source of delays is through the output where they result from hardware processing, through filter processing and also from delays in recording the exogenous input (a result of digital to analog conversions). Simulation studies can be used to investigate the effects of these delays on the controller and, more specifically, their effects on the ability of the H^∞ controller to reduce interior cavity pressure.

The uncertainties that enter through the exogenous input can be in the nature of amplitude errors, frequency errors or both. A rather extensive study of the uncertainties in the persistent input was undertaken and comparisons were made between amplitude-only errors, frequency-only errors and errors in both amplitude and frequency. These uncertainties can be incorporated as such into the governing equations of the model of the system. If this is done, the derivation of the feedback control gains through Algebraic Riccati Equations will be modified. One hopes, of course, that the improved controller will take into account these uncertainties and affect the compensator performance in a positive manner.

Another question of interest concerns the comparison of the standard LQG/Kalman filter with the H^∞/MinMax methodology, specifically in their effects on the performance of the closed loop system. The H^∞ methodology guarantees, in theory, a robustness bound but increases the computational and implementation complexity of the compensator. On the other hand the LQG/Kalman filter does not provide such a robustness bound but due to the simplicity of its structure appears more attractive from a practical point of view.

The numerical/algorithmic aspects of the H^∞ control implementation were studied extensively. In particular, the effects of the choice of the H^∞-norm bound, γ, on the suboptimal controller were investigated with computational simulations. Theoretically one can give a precise ratio of the H^∞ norm of the closed loop transfer function of the system designed utilizing an LQG/Kalman filter to that using the H^∞ formulation. As seen in [28], this depends on the number of invariant zeros (see [20], [23], [24], [25] for definition and extensive studies of the relationship between the "invariant" zeros and the properties of the

H^∞ controller). More precisely, in [28] Zhou showed that for the "one-block" system, this ratio of the norm of the transfer function of the system using the LQG/Kalman filter to that using the H^∞ methodology is no more than twice the number of the invariant zeros that lie in the right half plane. In the special case of minimum phase systems, the ratio is one. The extensions of these ideas to a "four-block" system (the type of the present structural acoustic system under study) reveal that this ratio is bounded by at least four times the order of the system. This unfortunately, does not shed any light, theoretically at least, in our comparison of the two control methodologies since the order of our original structural acoustics system is infinite. Even in the approximate system case (the numerical simulations were, of course, carried out using this system) the order is so large as to render these theoretical bounds useless. As we shall detail below, extensive simulations suggest that despite the lack of any theoretical bounds on this ratio, the performance of the LQG/Kalman filter (i.e the case where $\gamma = \infty$), is comparable to the H^∞ controller for our problem.

As we noted above, the tracking signal must be integrated even before the controller is applied to the system and this introduces a certain delay and increases the complexity of the system. One might consider ways in which to exclude this tracking signal from the controller computations. This can be done in at least two ways; first one might eliminate this tracking signal from the control law and also remove any information about the exogenous input from the state observer (we call this Case I). The other way (Case II) is to include all information of the exogenous signal in the state observer but exclude the tracking signal from the control law. Both cases were investigated numerically and compared to the case where the tracking signal was used in the control law and full information about the exogenous input was used in the state observer. The results of these calculations were rather surprising as we found the performance of each approach was *frequency-dependent*. For certain frequencies, controls based on Case I outperformed those from Case II while for other frequencies, the reverse was true. Furthermore, for some frequencies, the performance of both Case I and II was close to or worse than that of the open loop case. As might be expected, the performances in both cases were somewhat degraded when compared to the case where the tracking variable was included in the control law. If, depending on the frequency used, the approach of either case is to be used, there will be a compromise between the implementational ease of the controller application and reduced performance of such a controller.

By an extensive study of the computational and implementational aspects of the H^∞ controller applied to the acoustic-structure interaction model with piezoceramic actuators (a complex and large system by nature), the authors hope that they can provide some insight on H^∞ controller application to other large systems where theoretical results are not available. In the next section we give a description of the problem and model that served as a test example for the robustness computational studies of this paper.

2 A Structural Acoustic Noise Suppression Problem and its 2-D Approximation

A growing area of research in the structural acoustics community concerns the problem of reducing structure-borne noise levels within an acoustic cavity. A specific example of this is motivated by the development of a new class of turboprob and turbofan engines which are very fuel efficient but also very loud. The low frequency high magnitude acoustic fields produced by these engines cause vibrations in the fuselage which in turn generate unwanted interior noise. The passive control techniques which were initially employed to reduce the acoustic pressure levels were in general undesirable since the increased weight offset the advantages gained through the use of the new engines and lighter construction materials. This motivated the study of active control techniques for this problem both in a frequency domain setting and from a time domain approach (PDE approach).

In this section we describe a model for a structural acoustic test apparatus at NASA Langley Research Center. In collaboration with scientists (R. Silcox, D. Brown, V. Metcalf, H. Lester) from the Structural Acoustics Branch, NASA Langley Research Center, we have been using this device to test control methodologies described here and elsewhere (see [2, 3, 12, 14, 16]). The experimental apparatus consists of a rigid cylinder with a flexible plate at one end. Thus the domain Ω of interest consists of a cylinder of length ℓ and radius a as pictured in Figure 1. At one end of the cylinder is a flexible plate of thickness h which is assumed to have Kelvin-Voigt damping. It is also assumed that the edges of the plate are fixed. The other end of the cylinder is closed, and hardwall boundary conditions are assumed on all walls of the cylinder other than the flexible plate. The choice of this geometry and configuration results from the setup of the experimental apparatus which actually consists of a concrete pipe with a clamped aluminum plate at one end.

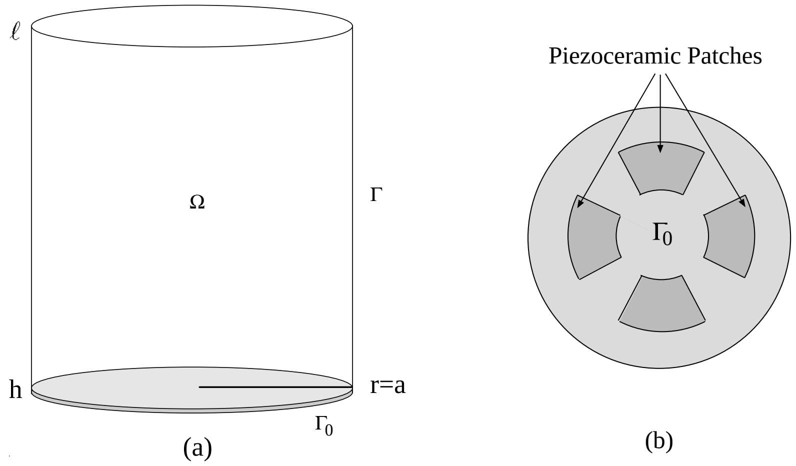

Figure 1. (a) The cylindrical acoustic cavity; (b) The circular plate with patches.

Control is implemented in the model via piezoceramic patches on the plate (see Figure 1b) which produce pure bending moments and/or extensional forces when a voltage is applied [17].

Because of the coupling between the interior acoustic field and the structural vibrations, this provides a means of controlling the interior acoustic pressure levels through the control of the dynamics of the bounding structure. The benefits of using the piezoceramic patches as actuators are augmented by the fact that they are inexpensive, lightweight and space efficient.

For acoustic waves having small amplitude, the cavity dynamics can be modeled by the undamped linear wave equation

$$\begin{aligned} \phi_{tt} &= c^2 \Delta\phi \qquad , \quad (r,\theta,z) \in \Omega \; , t > 0 \; , \\ \nabla\phi \cdot \hat{n} &= 0 \qquad , \quad (r,\theta,z) \in \Gamma \; , t > 0 \end{aligned}$$

where c is the speed of sound in the cavity, ϕ is the acoustic velocity potential, and the Laplacian in cylindrical coordinates is given by

$$\Delta\phi = \frac{\partial^2\phi}{\partial r^2} + \frac{1}{r}\frac{\partial\phi}{\partial r} + \frac{1}{r^2}\frac{\partial^2\phi}{\partial\theta^2} + \frac{\partial^2\phi}{\partial z^2} \; .$$

The boundary conditions on Γ (all walls other than the plate) model the hard wall conditions of the experimental concrete cylinder. Acoustic damping is omitted due to the relatively small dimensions of the cylinder ($a = 9\,in$, $\ell = 42\,in$). Finally, we point out that the acoustic pressure p is related to the potential through the relationship $p = \rho_f \phi_t$ where ρ_f is the equilibrium density of the interior cavity fluid (air).

The motion of the plate is influenced by a forcing function f which models the exterior noise source, the moments generated by the patches, and the backpressure due to pressure oscillations within the cavity. In formulating the patch contributions, we have assumed that s piezoceramic patches have been bonded to the plate as depicted in Figure 1. As detailed in [11], the strong form of the equations of motion for a fixed-edge, damped circular plate that is subjected to these moments and forces is

$$\begin{aligned} &\rho_p h w_{tt} + \frac{\partial^2 \mathcal{M}_r}{\partial r^2} + \frac{2}{r}\frac{\partial \mathcal{M}_r}{\partial r} - \frac{1}{r}\frac{\partial \mathcal{M}_\theta}{\partial r} + \frac{2}{r}\frac{\partial^2 \mathcal{M}_{r\theta}}{\partial r\partial\theta} + \frac{2}{r^2}\frac{\partial \mathcal{M}_{r\theta}}{\partial\theta} + \frac{1}{r^2}\frac{\partial^2 \mathcal{M}_\theta}{\partial\theta^2} \\ &\quad = -\rho_f \phi_t(t,r,\theta,w(t,r,\theta)) + f(t,r,\theta) \; , \\ &w(t,a,\theta) = \frac{\partial w}{\partial r}(t,a,\theta) = 0 \end{aligned}$$

where w is the transverse displacement and ρ_p is the density of the plate. The general moments are given by

$$\begin{aligned} \mathcal{M}_r &= M_r - (M_r)_{pe} \\ \mathcal{M}_\theta &= M_\theta - (M_\theta)_{pe} \\ \mathcal{M}_{r\theta} &= M_{r\theta} \end{aligned}$$

where

$$\begin{aligned} M_r &= D\left(\frac{\partial^2 w}{\partial r^2} + \frac{\nu}{r}\frac{\partial w}{\partial r} + \frac{\nu}{r^2}\frac{\partial^2 w}{\partial\theta^2}\right) + c_D\left(\frac{\partial^3 w}{\partial r^2\partial t} + \frac{\nu}{r}\frac{\partial^2 w}{\partial r\partial t} + \frac{\nu}{r^2}\frac{\partial^3 w}{\partial\theta^2\partial t}\right) \quad , \\ M_\theta &= D\left(\frac{1}{r}\frac{\partial w}{\partial r} + \frac{1}{r^2}\frac{\partial^2 w}{\partial\theta^2} + \nu\frac{\partial^2 w}{\partial r^2}\right) + c_D\left(\frac{1}{r}\frac{\partial^2 w}{\partial r\partial t} + \frac{1}{r^2}\frac{\partial^3 w}{\partial\theta^2\partial t} + \nu\frac{\partial^3 w}{\partial r^2\partial t}\right) \quad , \qquad (2.1) \\ M_{r\theta} &= D(1-\nu)\left(\frac{1}{r}\frac{\partial^2 w}{\partial r\partial\theta} - \frac{1}{r^2}\frac{\partial w}{\partial\theta}\right) + c_D(1-\nu)\left(\frac{1}{r}\frac{\partial^3 w}{\partial r\partial\theta\partial t} - \frac{1}{r^2}\frac{\partial^2 w}{\partial\theta\partial t}\right) \end{aligned}$$

are the internal plate moments, and

$$(M_r)_{pe} = (M_\theta)_{pe} = \sum_{i=1}^{s} \mathcal{K}_i u_i(t) \chi_i(r,\theta)$$

are the applied patch moments for patches located at $r_{i1} \leq r \leq r_{i2}, \theta_{i1} \leq \theta \leq \theta_{i2}$. With E denoting the Young's modulus, the parameters $D = \frac{Eh^3}{12(1-\nu^2)}$, c_D and ν represent the flexural rigidity, damping coefficient and Poisson's ratio for the plate. Here χ_i is the indicator characteristic function for the i^{th} patch region, $u_i(t)$ is the voltage into the i^{th} patch, and $\mathcal{K}_i$ is a parameter which depends on the geometry, piezoceramic and plate material properties, and piezoelectric strain constant (see [17] for details). The piezoceramic material parameters $\mathcal{K}_i, i = 1, \cdots, s$ as well as the plate parameters ρ_p, D, c_D and ν must ultimately be considered to be unknown and in actual applications are obtained using parameter estimation techniques.

The final coupling equation is the continuity of velocity condition

$$\frac{\partial \phi}{\partial z}(t,r,\theta,w(t,r,\theta)) = -w_t(t,r,\theta) \qquad , \quad (r,\theta) \in \Gamma_0 \ , \ t > 0$$

which results from the assumption that the plate is impenetrable to air. We note that both the backpressure and velocity (momentum) coupling conditions are in general nonlinear due to the fact that they occur on the surface of the plate.

Under the assumption of small displacements which is inherent in the Love-Kirchhoff plate formulation, these nonlinear coupling terms are replaced by their linear approximations which yields the approximate system model

$$\begin{aligned}
&\phi_{tt} = c^2 \Delta \phi \qquad , \quad (r,\theta,z) \in \Omega \ , t > 0 \ , \\
&\nabla \phi \cdot \hat{n} = 0 \qquad , \quad (r,\theta,z) \in \Gamma \ , t > 0 \ , \\
&\frac{\partial \phi}{\partial z}(t,r,\theta,0) = -w_t(t,r,\theta) \qquad , \quad (r,\theta) \in \Gamma_0 \ , \ t > 0 \ , \\
&\rho_p h w_{tt} + \frac{\partial^2 M_r}{\partial r^2} + \frac{2}{r}\frac{\partial M_r}{\partial r} - \frac{1}{r}\frac{\partial M_\theta}{\partial r} + \frac{2}{r}\frac{\partial^2 M_{r\theta}}{\partial r \partial \theta} + \frac{2}{r^2}\frac{\partial M_{r\theta}}{\partial \theta} + \frac{1}{r^2}\frac{\partial^2 M_\theta}{\partial \theta^2} \\
&\qquad = \frac{\partial^2 (M_r)_{pe}}{\partial r^2} + \frac{2}{r}\frac{\partial (M_r)_{pe}}{\partial r} - \frac{1}{r}\frac{\partial (M_\theta)_{pe}}{\partial r} + \frac{1}{r^2}\frac{\partial^2 (M_\theta)_{pe}}{\partial \theta^2} \\
&\qquad -\rho_f \phi_t(t,r,\theta,0) + f(t,r,\theta) \ , \\
&w(t,a,\theta) = \frac{\partial w}{\partial r}(t,a,\theta) = 0 \ , \\
&\phi(0,r,\theta,z) = \phi_0(r,\theta,z) \quad , \quad w(0,r,\theta) = w_0(r,\theta) \ , \\
&\phi_t(0,r,\theta,z) = \phi_1(r,\theta,z) \quad , \quad w_t(0,r,\theta) = w_1(r,\theta) \ .
\end{aligned} \tag{2.2}$$

In the system model (2.2), the plate and acoustic equations are in strong form which leads to difficulties in the control problem since it involves the differentiation of the Heaviside function and the Dirac delta which then yields an unbounded control input term. Moreover, because of the presence of and differing material properties of the piezoceramic patches, it is assumed that ρ_p, D, c_D and ν for the combined structure are piecewise constant in nature (see [18]). Hence these parameters will be expanded in terms of a Heaviside basis with the edges of the patches defining the support of the basis functions. This also leads to problems in the strong form, however, since it necessitates the differentiation of discontinuous material parameters. To avoid these difficulties, it is advantageous to formulate the problem in a weak or variational form.

To provide classes of functions which are considered when defining a variational form of the problem, we consider the state space $X = \bar{L}^2(\Omega) \times L^2(\Gamma_0)$ and space of test functions $V = \bar{H}^1(\Omega) \times H_0^2(\Gamma_0)$ where $H_0^2(\Gamma_0) = \{\psi \in H^2(\Gamma_0) : \psi = \psi_r = 0 \text{ at r = a}\}$. Here $\bar{L}^2(\Omega)$ and $\bar{H}^1(\Omega)$ are the quotient spaces of L^2 and H^1 over the constant functions (the use of these spaces is due to the fact that the potentials are determined only up to a constant).

As discussed in [8, 10, 26], an appropriate linearized variational (energy) form of the coupled system equations modeling this setup is

$$\int_\Omega \frac{\rho_f}{c^2}\phi_{tt}\overline{\xi}d\omega + \int_\Omega \rho_f \nabla\phi \cdot \overline{\nabla\xi}d\omega \tag{2.3a}$$

$$+\int_{\Gamma_0} \rho_p h w_{tt}\overline{\eta}d\gamma + \int_{\Gamma_0} M_r\overline{\eta_{rr}}d\gamma + \int_{\Gamma_0} \frac{1}{r}M_\theta\overline{\eta_r}d\gamma + \int_{\Gamma_0} \frac{1}{r^2}M_{r\theta}\overline{\eta_{\theta\theta}}d\gamma \tag{2.3b}$$

$$+2\int_{\Gamma_0} \frac{1}{r}M_{r\theta}\overline{\eta_{r\theta}}d\gamma - 2\int_{\Gamma_0} \frac{1}{r^2}M_{r\theta}\overline{\eta_\theta}d\gamma$$

$$+\int_{\Gamma_0} \rho_f\left(\phi_t\overline{\eta} - w_t\overline{\xi}\right)d\gamma \tag{2.3c}$$

$$= \int_{\Gamma_0} \sum_{i=1}^{s} \mathcal{K}_i^B u_i(t)\left[H_{i1}(r) - H_{i2}(r)\right]\left[H_{i1}(\theta) - H_{i2}(\theta)\right]\overline{\nabla^2\eta}d\gamma + \int_{\Gamma_0} f\overline{\eta}d\gamma \tag{2.3d}$$

for all test functions $(\xi, \eta) \in V$ (note that $d\omega = r\,dr\,d\theta\,dz$ and $d\gamma = r\,dr\,d\theta$; the overbars in (2.3) denote complex conjugates).

As shown in [11], it is possible to write initial value problems for (2.3) in the form

$$\begin{aligned} \dot{y}(t) &= \mathcal{A}y(t) + \mathcal{B}u(t) + \mathcal{F}(t) \quad \text{in } \mathcal{V}^* \\ y(0) &= y_0. \end{aligned} \tag{2.4}$$

Here $y(t) = (\phi(t,\cdot), w(t,\cdot), \phi_t(t,\cdot), w_t(t,\cdot))$ is the state in $\mathcal{V} = V \times V$ with $\mathcal{V} \hookrightarrow \mathcal{H} \hookrightarrow \mathcal{V}^*$ forming a Gelfand triple with pivot space $\mathcal{H} = V \times X$. For details regarding well posedness, see [6, 11].

To approximate the system dynamics, Fourier-Galerkin schemes are used to discretize the infinite dimensional system (2.3). More specifically, the plate displacement is approximated by

$$w^{\mathcal{N}}(t,r,\theta) = \sum_{n=1}^{\mathcal{N}} w_n^{\mathcal{N}}(t)B_n^{\mathcal{N}}(r,\theta) \tag{2.5}$$

where $B_n^{\mathcal{N}}(r,\theta)$ are cubic spline/Fourier basis functions (see [10, 11, 26] for details). Similarly, the acoustic potential is approximated by

$$\phi^{\mathcal{M}}(t,r,\theta,z) = \sum_{m=1}^{\mathcal{M}} \phi_m^{\mathcal{M}}(t)P_m(r,\theta,z) \tag{2.6}$$

where in this case, $P_m(r,\theta,z)$ is a Legendre polynomial/Fourier basis element.

The substitution of the expansions (2.5) and (2.6) into (2.3) with individual basis elements chosen as the test functions in the usual Galerkin or finite element formulation yields the matrix system

$$\begin{aligned} \dot{y}^{\mathcal{P}}(t) &= A^{\mathcal{P}} y^{\mathcal{P}}(t) + B^{\mathcal{P}} u(t) + F^{\mathcal{P}}(t) \\ y^{\mathcal{P}}(0) &= y_0^{\mathcal{P}} \end{aligned} \tag{2.7}$$

where $\mathcal{P} = 2(\mathcal{M} + \mathcal{N})$ and $y^{\mathcal{P}}$ contains the generalized Fourier coefficients for the approximate plate displacement and acoustic potential as well as their temporal derivatives (again, see [10, 26] for details concerning the discretization of the system equations and formulation of the matrices $A^{\mathcal{P}}, B^{\mathcal{P}}$ and $F^{\mathcal{P}}$). In this form, the finite dimensional control problem can be formulated.

Before describing the control problem, we discuss briefly a 2-D structural acoustics model problem that has proved useful in many of our previous efforts. If one takes a longitudinal "slice" as pictured in Figure 2, the problem described above becomes a 2-D acoustic cavity with a 1-D flexible boundary for the interacting structure. (This is essentially equivalent to assuming that one has uniformity in the direction perpendicular to the "slice".)

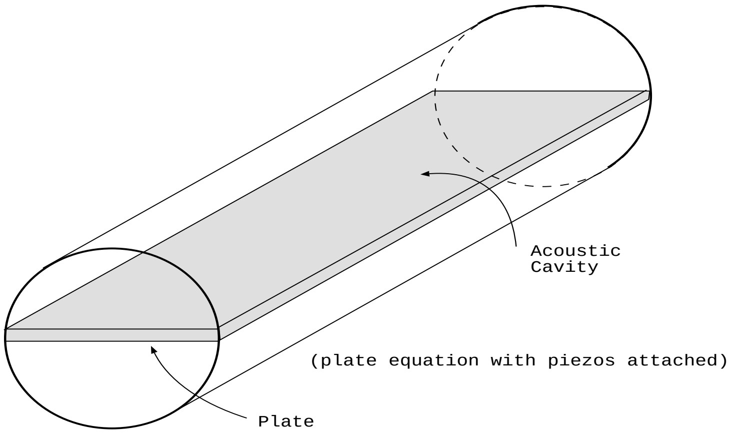

Figure 2. 2-D "slice" of the cylindrical acoustic cavity.

The moving plate reduces to a flexible beam (Euler-Bernoulli with Kelvin-Voigt damping), as depicted in Figure 3(b), while the pressure field in the cavity, as presented in Figure 3(a), is described by a 2-D version of the acoustic wave equation. The coupling terms are essentially the same. This 2-D coupled model has been developed and analyzed (both theoretically and computationally) in our earlier work [4]. We have found that it is an excellent reduced dimension model to use in computational control and identification investigations (see, for example, [5, 9, 12, 13]) since we are able to use findings from tests with this model to accurately predict the 3-D model responses and to anticipate implementation difficulties in the feedback control algorithms. It is for this reason that we have used the reduced dimension model in all of the calculations reported in this paper.

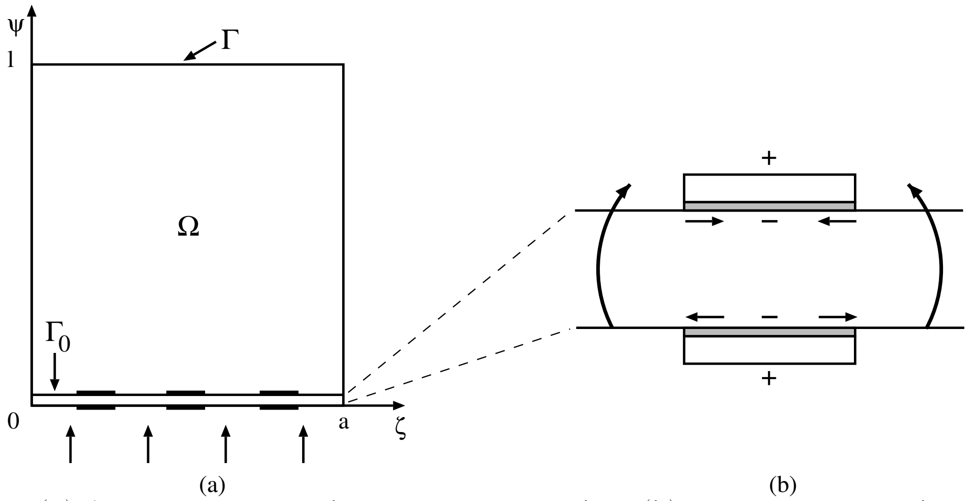

Figure 3. (a) Acoustic cavity with piezoceramic patches, (b) Piezoceramic patch excitation.

3 Control Methodology

We now outline a methodology for an H^∞/MinMax periodic control of structural acoustic problems and its finite dimensional implementation. For brevity, we suppress the finite dimensional indexing (i.e. the $\mathcal{P}$ in (2.7)) of vectors and matrices and adopt notation similar to that for the infinite dimensional model with the understanding that it is the finite dimensional approximate model that is intended. In the rest of this note we will refer to the 2-D model since it is this reduced dimension model that has been used in our computational efforts. Here it is assumed that the only external moments and forces being applied to the beam are the external periodic forces applied to the beam having a period τ and hence $F(0) = F(\tau)$ in (2.7). The above case is used to model the structural acoustic system when it is subjected to a periodic exterior acoustic field. We consider the system (in the form given in the equation above, (2.7)) with the periodic external force $F(t)$ and an added disturbance (error) input denoted by $\eta(t)$, thus giving

$$\begin{aligned} \dot{y}(t) &= Ay(t) + Bu(t) + D\eta(t) + F(t) \\ y(0) &= y_0 \end{aligned} \tag{3.1}$$

with $y(0) = y(\tau)$. The performance output $z(t) \in Z$ is given by

$$z(t) = Hy(t) + Gu(t), \tag{3.2}$$

where Z is a performance output space and $H : \mathcal{H} \to Z$, $G : U \to Z$. The disturbance evolves in a space W and it is assumed that $D : W \to \mathcal{H}$ with $H^*G = 0$. For the finite dimensional approximate system, the problem of determining a controlling voltage can then be posed as the problem of finding $u \in L^2(0, \tau; U)$ which minimizes the steady-state disturbance-augmented functional (or, equivalently, the "soft-constrained" disturbance attenuation index)

$$J(u) = \int_0^\tau \left\{ \langle Qy(t), y(t)\rangle_{R^p} + \langle Ru(t), u(t)\rangle_{R^s} - \gamma^2 |\eta(t)|_W^2 \right\} dt$$

where $y(t)$ solves (3.1) and R is an $s \times s$ diagonal matrix containing weights which penalize overly large voltages to the patches (this ensures that realistic voltages are determined). As seen in [5], energy considerations suggest that a diagonal matrix multiple of the mass matrix is an appropriate choice for the nonnegative matrix Q. Here $\gamma \in \mathbb{R}$ is a fixed positive constant which is a design parameter to be chosen as small as possible. In this case, the H^∞ norm of the closed loop disturbance to performance output transfer function from $\eta(\cdot)$ to $z(\cdot)$ is bounded above by γ. Under suitable conditions, optimal control theory can then be used to show that the optimal controlling voltage is given by

$$u(t) = -Ky(t) + R^{-1}(B)^T r(t) \tag{3.3}$$

where $K = R^{-1}(B)^T\Pi$ and Π is the unique nonnegative self adjoint solution to the (H^∞-control) algebraic Riccati equation

$$(A)^T\Pi + \Pi A - \Pi\left(BR^{-1}(B)^T - \frac{1}{\gamma^2}D(D)^T\right)\Pi + Q = 0\ . \tag{3.4}$$

The tracking component $r(t)$ solves the linear differential equation

$$\begin{aligned} \dot{r}(t) &= -\left[A - \left(BR^{-1}(B)^T - \tfrac{1}{\gamma^2}D(D)^T\right)\Pi\right]^T r(t) + \Pi F(t) \\ r(0) &= r(\tau)\ . \end{aligned} \tag{3.5}$$

A disadvantage to the feedback law (3.3) above, is that it requires knowledge of the full state (displacement, velocity, potential and pressure) in order to be implemented. In reality, however, the system response is measured only at a small number of discrete locations on the plate and in the cavity and from these values, one must reconstruct or estimate the state before using it to determine the controlling voltage [1, 4, 16]. This yields a feedback law of the form

$$u(t) = -Ky_c(t) + R^{-1}(B)^T r(t) \tag{3.6}$$

where $r(t)$ is again the unique τ-periodic solution of (3.5), $y_c(t)$ solves the H^∞-state estimator or compensator equation

$$\begin{aligned} \dot{y}_c(t) &= \left[A - F_cC - BK + \frac{1}{\gamma^2}D(D)^T\Pi\right]y_c(t) + F_c y_{ob}(t) \\ &\qquad + F(t) + \left(BR^{-1}(B)^T - \frac{1}{\gamma^2}D(D)^T\right)r(t) \\ y_c(0) &= y_{c0} \end{aligned} \tag{3.7}$$

(compare to the original finite dimensional system (3.1) with the expression (3.6) for the voltage). Here C is a matrix specifying the points where data is observed. The matrix F_c has a form similar to that of the gain K and is given by $F_c = (I - \frac{1}{\gamma^2}\Sigma\Pi)^{-1}\Sigma(C)^T\mathcal{N}_e^{-1}$ where $\mathcal{N}_e$ is a design matrix which is related to the effect of noise in the data and Σ solves a second algebraic Riccati equation

$$A\Sigma + \Sigma(A)^T - \Sigma\left((C)^T\mathcal{N}_e^{-1}C - \frac{1}{\gamma^2}Q\right)\Sigma + D(D)^T = 0. \tag{3.8}$$

In addition to the self adjointness of the matrices Π and Σ, a supplementary condition is imposed, namely the boundedness of the spectral radius of $\Sigma\Pi$ by γ^2, see [1, 21, 27];

consequently this coupling equation reads

$$r_{sp}(\Sigma\Pi) < \gamma^2. \tag{3.9}$$

In these finite dimensional simulations, the vector $y_{ob}(t)$ contains the generalized Fourier coefficients for the observed state and it is from this information that the state is approximated; it is given by

$$y_{ob}(t) = Cy(t) + E\eta(t), \tag{3.10}$$

where the matrix $\mathcal{N}_e$ takes the specific form

$$\mathcal{N}_e = E(E)^T$$

with $\mathcal{N}_e$ invertible and satisfies $DE^T = 0$, see [1, 19, 21, 22]. In order to satisfy the condition $DE = 0$ which would maintain certain symmetry (see [1]), and guaranteee that the disturbance signal for the state (entering through the term $D\eta(t)$) and the output signal disturbance (entering though the signal $E\eta(t)$) be independent, we could have chosen

$$D_{new} = [D \quad 0] \qquad E_{new} = [0 \quad E],$$

which results in $D_{new}E^T_{new} \equiv 0$. Instead, we considered the case where the term $D\eta(t)$ (3.1) is given by $D\eta_1(t)$ and the term $E\eta(t)$ in (3.7) is given by $E\eta_2(t)$, with $\eta_1(t)$ and $\eta_2(t)$ independent, (see [1, 4, 21, 22]).

4 Implementation of Approximated 2-D System

We briefly describe the Galerkin approximation scheme used to approximate the beam/cavity system. Our scheme for the first order formulation of the approximated system (3.1) was of dimension $\mathcal{P}$ where $\mathcal{P} = 2(m + n - 1)$ with $n-1$ modified cubic splines used for the beam approximation and m tensor products of Legendre polynomials used for the cavity approximation (see [5] for complete details).

We let $\{B_i^n\}_{i=1}^{n-1}$ denote the 1-D cubic spline basis functions which are used to discretize the beam and let $\{B_i^m\}_{i=1}^m$ denote the 2-D Legendre basis functions which are used to discretize the cavity. The $n-1$ and m dimensional subspaces are taken to be span$\{B_i^n\}_{i=1}^{n-1}$ and span$\{B_i^m\}_{i=1}^m$, respectively. The approximating state space is $X^N = \text{span}\{B_i^n\}_{i=1}^{n-1} \times \text{span}\{B_i^m\}_{i=1}^m$ and the product space for the first order system (3.1) is $\mathcal{H}^{\mathcal{P}} = X^N \times X^N$. When the approximate beam and cavity solutions (of the 2-D "slice" of the reduced system (2.2)) are taken to be

$$w^N(t,\zeta) = \sum_{i=1}^{n-1} w_i^N(t) B_i^n(\zeta) \quad \text{and} \quad \phi^N(t,\zeta,\psi) = \sum_{i=1}^{m} \phi_i^N(t) B_i^m(\zeta,\psi),$$

respectively, this yields the (finite dimensional first order) system

$$M\dot{y}(t) = \tilde{A}y(t) + \tilde{B}u(t) + \tilde{D}\eta_1(t) + \tilde{F}(t),$$

$$My(0) = \tilde{y}_0,$$

$$y_{ob}(t) = Cy(t) + E\eta_2(t),$$

where

$$y(t) = \begin{pmatrix} \vartheta(t) \\ \dot{\vartheta}(t) \end{pmatrix}.$$

Here

$$\vartheta(t) = \left[\begin{array}{cccccc} \phi_1^N(t) & \dots & \phi_m^N(t) & w_1^N(t) & \dots & w_{n-1}^N(t) \end{array} \right],$$

contains the $N \times 1 = (m+n-1) \times 1$ approximate state vector coefficients. The full system has the form

$$\begin{aligned} \begin{bmatrix} M_1 & 0 \\ 0 & M_2 \end{bmatrix} \begin{bmatrix} \dot{\vartheta}(t) \\ \ddot{\vartheta}(t) \end{bmatrix} &= \begin{bmatrix} 0 & M_1 \\ -A_1 & -A_2 \end{bmatrix} \begin{bmatrix} \vartheta(t) \\ \dot{\vartheta}(t) \end{bmatrix} + \begin{bmatrix} 0 \\ \tilde{B} \end{bmatrix} u(t) \\ &+ \begin{bmatrix} \tilde{D}_1 & 0 \\ 0 & \tilde{D}_2 \end{bmatrix} \eta_1(t) + \begin{bmatrix} 0 \\ \tilde{F}(t) \end{bmatrix}, \end{aligned}$$

$$y_{obs}(t) = C \begin{bmatrix} \vartheta(t) \\ \dot{\vartheta}(t) \end{bmatrix} + E\eta_2(t),$$

$$\begin{bmatrix} M_1 & 0 \\ 0 & M_2 \end{bmatrix} \begin{bmatrix} \vartheta(0) \\ \dot{\vartheta}(0) \end{bmatrix} = \begin{bmatrix} g_1 \\ g_2 \end{bmatrix},$$

with

$$M_1 = \operatorname{diag}[M_{11}, M_{12}], \quad M_2 = \operatorname{diag}[M_{21}, M_{22}],$$

$$A_1 = \operatorname{diag}[A_{11}, A_{12}], \quad A_2 = \begin{bmatrix} 0 & A_{31} \\ A_{32} & A_{22} \end{bmatrix},$$

and

$$\tilde{B} = \begin{bmatrix} 0 \\ \tilde{B}_2 \end{bmatrix}, \quad \tilde{F} = \begin{bmatrix} 0 \\ \tilde{F}_2(t) \end{bmatrix}.$$

For this specific system, the term $\tilde{D}\eta_1(t)$ is given by

$$\tilde{D}\eta_1(t) = \begin{bmatrix} \tilde{D}_1 & 0 \\ 0 & \tilde{D}_2 \end{bmatrix} \cdot \eta_1(t) = \begin{bmatrix} \left[\tilde{D}_{11}\right]_l & 0 & 0 & 0 \\ 0 & \left[\tilde{D}_{12}\right]_p & 0 & 0 \\ 0 & 0 & \left[\tilde{D}_{21}\right]_l & 0 \\ 0 & 0 & 0 & \left[\tilde{D}_{22}\right]_p \end{bmatrix} \cdot \eta_1(t)$$

$$
= \begin{bmatrix} \left(\int_\Omega 1.0 \cdot \nabla B_l^m d\omega\right) \cdot \eta_{1\phi}(t), & l = 1, \ldots, m, \\ \left(\int_{\Gamma_0} 1.0 \cdot D^2 B_p^n d\gamma\right) \cdot \eta_{1w}(t), & p = 1, \ldots, n-1, \\ \left(\frac{\rho_f}{c^2} \int_\Omega 1.0 \cdot B_l^m d\omega\right) \cdot \eta_{1\phi_t}(t), & l = 1, \ldots, m, \\ \left(\rho_b \int_{\Gamma_0} 1.0 \cdot B_p^n d\gamma\right) \cdot \eta_{1w_t}(t), & p = 1, \ldots, n-1, \end{bmatrix},
$$

where

$$
\eta_{1\phi}(t) = 0,
$$

$$
\eta_{1w}(t) = 0,
$$

$$
\eta_{1\phi_t}(t) = \max_{t \in [t_0, t_f]}\{\rho_f \phi_t(t, \zeta, \psi)_{OL}\} \cdot \alpha_1(t),
$$

$$
\eta_{1w_t}(t) = \max_{t \in [t_0, t_f]}\{w_t(t, \zeta)_{OL}\} \cdot \alpha_1(t)
$$

and $\alpha_1(t)$ is a random number on $[0, 1]$ with uniform distribution.

If it is assumed that m_{out} outputs are used, then the $m_{out} \times \mathcal{P}$ matrix C is given by

$$
C \begin{bmatrix} \phi^N(t) \\ w^N(t) \\ \dot{\phi}^N(t) \\ \dot{w}^N(t) \end{bmatrix} = \begin{bmatrix} 0 & 0 & 0 & 0 \\ 0 & [C_{displ}] & 0 & 0 \\ 0 & 0 & [C_{press}] & 0 \\ 0 & 0 & 0 & [C_{vel}] \end{bmatrix} \begin{bmatrix} \phi(t) \\ w(t) \\ \phi_t(t) \\ w_t(t) \end{bmatrix},
$$

with

$$
[C_{displ}] = \left[\ C_{displ}^{i_d}\ \right]_{i_d} = \left[\ \int_{\Gamma_0} \delta(\zeta - \zeta_{i_d}) B_{k_d}^n(\zeta) d\zeta\ \right]_{i_d} = \left[\ B_{k_d}^n(\zeta_{i_d})\ \right],
$$

$$
[C_{press}] = \left[\ C_{press}^{i_p}\ \right]_{i_p} = \left[\ \rho_f \int_\Omega \delta(\zeta - \zeta_{i_p}, \psi - \psi_{i_p}) B_{k_p}^m(\zeta, \psi) d\omega\ \right]_{i_p} = \left[\ \rho_f B_{k_p}^m(\zeta_{i_p}, \psi_{i_p}\ \right],
$$

$$
[C_{vel}] = \left[\ C_{vel}^{i_v}\ \right]_{i_v} = \left[\ \int_{\Gamma_0} \delta(\zeta - \zeta_{i_v}) B_{k_v}^n(\zeta) d\zeta\ \right] = \left[\ B_{k_v}^n(\zeta_{i_v})\ \right],
$$

where $\delta(\zeta - \zeta_i)$ and $\delta(\zeta - \zeta_i, \psi - \psi_i)$ are the one and two dimensional Dirac delta functions, respectively, and $k_d = 1, \ldots, n-1$, $i_d = 1, \ldots, n_{displ}$, $k_p = 1, \ldots, m$, $i_p = 1, \ldots, n_{mic}$,

$k_v = 1, \ldots, n-1, \;\; i_v = 1, \ldots, n_{vel}$. The $m_{out} \times m_{out}$ matrix E is given by

$$E\eta_2(t) = \begin{bmatrix} 1 & \cdots & 0 \\ \vdots & \ddots & \vdots \\ 0 & \cdots & 1 \end{bmatrix} \left(\begin{bmatrix} e_1 \\ \vdots \\ e_{m_{out}} \end{bmatrix} \alpha_2(t) \right) = \begin{bmatrix} \max_t\{w(t,\zeta_1)_{OL}\} \\ \vdots \\ \max_t\{w(t,\zeta_{n_{displ}})_{OL}\} \\ \max_t\{\rho_f \phi_t(t,\zeta_1,\psi_1)_{OL}\} \\ \vdots \\ \max_t\{\rho_f \phi_t(t,\zeta_{n_{mic}},\psi_{n_{mic}})_{OL}\} \\ \max_t\{w_t(t,\zeta_1)_{OL}\} \\ \vdots \\ \max_t\{w_t(t,\zeta_{n_{vel}})_{OL}\} \end{bmatrix} \alpha_2(t)$$

where $\alpha_2(t)$ is a random number with uniform distribution on $[0,1]$. The initial conditions given by the vectors $g_1 = [g_{11}, g_{12}]$ and $g_2 = [g_{21}, g_{22}]$ have elements

$$g_{11} = \int_\Omega \nabla\phi_0 \cdot \nabla B_l^m \, d\omega, \qquad g_{12} = \int_{\Gamma_0} D^2 w_0 \cdot D^2 B_p^n \, d\gamma,$$
$$g_{21} = \frac{\rho_f}{c^2} \int_\Omega \phi_1 \cdot B_l^m \, d\omega, \qquad g_{22} = \rho_b \int_{\Gamma_0} w_1 \cdot B_p^n \, d\gamma,$$

The system can now be written as a set of $2\mathcal{P}$ ordinary differential equations given by tha plant equation (3.1) and the state estimator equation (3.7), where $A = (M)^{-1}\tilde{A}$, $B = (M)^{-1}\tilde{B}$, $D = (M)^{-1}\tilde{D}$, $F = (M)^{-1}\tilde{F}$, $y_0 = (M)^{-1}\tilde{y}_0$, and $y_{c_0} = (M)^{-1}\tilde{y}_{c_0}$. Furthermore, the matrices Π and Σ are solutions to the algebraic matrix Riccati equations (3.4) and (3.8) that satisfy the coupling equation (3.9). Because of energy considerations (see, [5]), a suitable choice for the matrix Q is

$$Q = \Delta \begin{bmatrix} M_1 & 0 \\ 0 & M_2 \end{bmatrix},$$

where the diagonal matrix Δ is given by

$$\Delta = \mathrm{diag}\,[d_1 I^m, d_2 I^{n-1}, d_3 I^m, d_4 I^{n-1}].$$

As it was pointed out in [5, 12], with the above choice for Q, the first inner product in the definition of $J(u)$ simplifies to

$$\begin{aligned} \langle Qy(t), y(t)\rangle_{\mathcal{H}} &= d_1 \int_\Omega |\nabla\phi|^2 d\omega + d_2 \int_{\Gamma_0} \left(D^2 w\right)^2 d\gamma \\ &+ d_3 \int_\Omega \frac{\rho_f}{c^2} \left(\dot{\phi}\right)^2 d\omega + d_4 \int_{\Gamma_0} \rho_b \,(\dot{w})^2 \, d\gamma. \end{aligned}$$

This in essence minimizes the finite dimensional approximations to the kinetic and potential energies of the undamped beam and wave equation, [5].

Machine Specifications: As one might well expect, the desired weighting for the design components of the D matrix is intimately related to the numerical stability of the solutions to the two Riccati equations. From extensive studies on the numerical behavior of the condition numbers of the two Riccati solutions, it was observed that these solutions (condition numbers) depended heavily on the weighting of the matrices D, Q, R, and $\mathcal{N}$ and the parameter γ. Acceptable condition numbers for Π were $\sim 10^{16}$ and for Σ were $\sim 10^{18}$. These were actually the best (smallest) condition numbers achieved with any weighting of the four matrices. Our preliminary calculations were performed on an IBM RISCSystem/6000 250 using double precision arithmetic. We point out that although the above condition numbers lie at the limits of double precision arithmetic, extensive numerical tests indicated consistent results and acceptable relative errors in the Riccati solutions. Moreover, good control results were obtained with these solutions. Hence we did not appear to be losing significant information in spite of the large condition numbers for the Riccati solutions.

5 Description of Numerical Studies

Below, we summarize the procedure for the numerical studies mentioned in Section 1 and reported in the next section.

Frequency Uncertainties. As a first study, which is Example 1 of Section 6, we considered the effects of frequency and/or amplitude uncertainties in the exogenous signal, F. This signal is assumed to be the sum of a nominal term F_0, which is known, and a perturbation ΔF, which is unknown. This perturbation accounts for uncertainties in the exterior noise field due to limitations in measurement equipment, delays due to hardware, et cetera. We design the state estimator based on the nominal term F_0, and use this nominal term in both the state estimator equation (3.7) and the tracking component (3.5).

In the numerical studies, we first introduced frequency uncertainties ($\Delta F \neq 0$) in the exogenous signal that appears in the state equation but used only the nominal part F_0 of this signal in the state observer and tracking filter equations, (3.7) and (3.5). We observed that for small frequency errors of the tracking signal, the performance of the H^∞ compensator and that of the full state H^∞ controller are comparable. However both give unsatisfactory results for higher frequency errors.

In the second part of this study, we included the perturbation of the exogenous input into the uncertainty term $D\eta(t)$ giving a new uncertainty term

$$\tilde{D}\tilde{\eta}(t) = D\eta(t) + \Delta F(t) = [D \quad I_f] \begin{bmatrix} \eta(t) \\ \Delta F(t) \end{bmatrix}. \tag{5.1}$$

The frequency and amplitude uncertainties of the exogenous signal were therefore incorporated in the controller design via the controller gains (modified D term in the algebraic Riccati equation solutions), thus affecting the controller structure. As expected, amplitude uncertainties can be tolerated whereas frequency uncertainties result in unacceptable performance. With the uncertainties (amplitude and frequency) incorporated into the controller, we see no improvement in comparison to the case when the uncertainties were excluded from the controller structure (first part of this study).

Remark 1 *The operator I_f in* (5.1) *is not quite the identity operator. Actually it is the "identity" for the beam velocity component. Its finite dimensional approximation is given by*

$$I_f \equiv \begin{bmatrix} 0 \\ 0 \\ 0 \\ M_{22}^{-1} \cdot \int_{\Gamma_0} 1 \cdot B_p^n \, d\gamma \end{bmatrix}$$

where the mass matrix M_{22} is given in [5].

Remark 2 *Recalling the finite dimensional approximations of the terms $D\eta_1(t)$ and $F(t)$ from §4 (see [4] for a detailed description), we have*

$$D\eta_1(t) = \begin{bmatrix} d_{11} & 0 & 0 & 0 \\ 0 & d_{12} & 0 & 0 \\ 0 & 0 & d_{13} & 0 \\ 0 & 0 & 0 & d_{14} \end{bmatrix} \cdot \begin{bmatrix} \eta_{1\phi}(t) \\ \eta_{1w}(t) \\ \eta_{1\dot{\phi}}(t) \\ \eta_{1\dot{w}}(t) \end{bmatrix}, \quad \textit{where} \quad \begin{aligned} d_{11} &= M_{11}^{-1} \int_{\Omega} 1 \cdot \nabla B_l^m \, d\omega \\ d_{12} &= M_{12}^{-1} \int_{\Gamma_0} 1 \cdot D^2 B_p^n \, d\gamma \\ d_{13} &= M_{21}^{-1} \int_{\Omega} 1 \cdot B_l^m \, d\omega \\ d_{14} &= M_{22}^{-1} \int_{\Gamma_0} 1 \cdot B_p^n \, d\gamma \end{aligned}$$

and

$$I_f \cdot \Delta F(t) = \begin{bmatrix} 0 \\ 0 \\ 0 \\ M_{22}^{-1} \cdot \int_{\Gamma_0} 1 \cdot B_p^n \, d\gamma \end{bmatrix} \cdot \Delta f(t)$$

which, when combined together, yield the new term for $D\eta_1(t)$, namely

$$\tilde{D}\tilde{\eta}_1(t) = \begin{bmatrix} d_{11} & 0 & 0 & 0 & 0 \\ 0 & d_{12} & 0 & 0 & 0 \\ 0 & 0 & d_{13} & 0 & 0 \\ 0 & 0 & 0 & d_{14} & I_f \end{bmatrix} \cdot \begin{bmatrix} \eta_{1\phi}(t) \\ \eta_{1w}(t) \\ \eta_{1\dot{\phi}}(t) \\ \eta_{1\dot{w}}(t) \\ \Delta F(t) \end{bmatrix}.$$

It should be noted that the first two terms of $\eta_1(t)$, namely $\eta_{1\phi}(t)$ and $\eta_{1w}(t)$, are set to zero. The reason is that the components d_{11} and d_{12} are assigned a nonzero value to improve the conditioning of the Riccati solutions (3.4) *and* (3.8), *and therefore with $\eta_{1\phi}(t) = \eta_{1w}(t) = 0$, their product would still yield zero in the first two components of $D\eta_1(t)$ of the state equation* (3.1).

Time delays. An extensive study was undertaken in the second example of Section 6 to determine how the time delays and discrete time approximations affect the performance of the controller. Time delays were inserted (a) in the plant output (3.10), which was used in the state estimator equation, (b) in the input voltage (3.6), which was used only by the plant since the state estimator can readily use the computer generated input voltage (both are software generated), and (c) in the forcing signal (exogenous signal F) which was only applied to the plant. Each of these simulate a possible case of delays in actual implementation of the feedback control algorithms. When degradation occurs due to a particular type of delay, one must take extra precaution to reduce this delay in implementation whenever possible.

We observed that the closed loop system for this process can handle time delays in the forcing function F and can tolerate very small delays in the measured output (3.10). It becomes unstable however, for any delays in the input voltage (3.6). For a small time delay, specifically 1/2 time delay which corresponds to $\approx 11.2^o$ phase delay, we made an additional study of the delay contributions of the components of the input voltage. As seen in Example 2, much of the performance degradation from the (delayed) voltage signal is due to delays in the state estimator signal, $y_c(t)$. However, delays in the tracking variable $r(t)$ also contribute to significant degradation.

$\mathbf{H}^\infty$ vs LQG. A comparison of the standard LQG/Kalman filter ($\gamma = \infty$) and the H^∞ compensator was undertaken in Example 3 of Section 5. In this comparison we varied the bound from $\gamma = 1.7$ (the smallest value guaranteeing a solution of the Riccati equations, (3.4) and (3.8)) up to $\gamma = \infty$ (Kalman filter). In addition to considering the theoretical aspect of this comparison, we also looked at the numerical effects of the two control methodologies. Specifically, we focused on the condition numbers of the two Riccati equations and the spectral radius of their product, (see equation (3.9)). Furthermore, we considered the sound pressure level at a specific point inside the cavity. This revealed no significant differences between the two methodologies.

Tracking Filter. The last test deals with the effects of the tracking variable $r(t)$. One possibility is to remove the tracking signal $r(t)$ from the control law and eliminate all information about the exogenous input from the state estimator equation, i.e $r = 0$ in (3.6) and $F = 0, r = 0$ in (3.7); this is referred to as Case I here and below. This choice would drastically reduce the complexity of the control law and eliminate possible delays in the implementation of such a control law. Another scenario, denoted below as Case II, excludes the tracking variable from the control law (which introduces delays in the implementation of the control law by the use of the backward in time integration), *but* includes all information of the exogenous signal $F(t)$ in the state estimator equation, i.e. $r = 0$ in (3.6), $F \neq 0, r = 0$ in (3.7). The above two cases were also compared to the case where the tracking signal and associated variables were included fully in the control law (called the ideal case). In each of the three cases, we looked at the sound pressure level at various cavity points, the rms displacement and rms velocity at various points along the beam, and the rms input voltage. The results showed that performance is frequency-dependent for both Case I and Case II, with none outperforming the ideal case.

The extensive study on the implementational aspects of the H^∞ compensator illustrated that the controller design can handle uncertainties in the exogenous signal amplitude. However, only zero or infinitesimal uncertainties in the exogenous signal frequency can be tolerated in this system. The study also discloses that the H^∞ methodology gives some robustness in the presence of the amplitude uncertainties. It was observed however, that for this system, time delays in the input signal are not adequately handled by either the LQG or H^∞ controllers. In the case of time delays in the tracking signal, some delays can be handled without affecting the overall performance of the compensator.

A compromise between the implementational ease of the controller application and the reduced performance of the controller exists when information about the tracking variable is omitted from the control law, and the performance of the controller in this case is frequency-dependent. This compromise introduces the additional burden on the design engineers to have an a-priori knowledge of the exact tracking signal frequency. The comparison between the standard LQG/Kalman filter and the H^∞ compensator exhibited no significant differences. This absence of significant difference in performance is quite attractive from an implementational and theoretical point of view, since it simplifies the structure of the control law and does not require computationally intensive numerical calculations for the derivation of the controller gains (algebraic Riccati solutions). This performance similarity has even more importance in the 3-D structural acoustics model where the dimension of the approximate system increases drastically and any reduction in calculation would affect (improve) the overall performance of the controller.

6 Numerical Results

For all the simulation studies below, we used a space discretization index $\mathcal{P} = 110$ (see (2.5) - (2.7)) for the approximate plant equation (3.1) and compensator equation (3.7), as well as the tracking signal equation (3.5).

6.1 Example 1: Frequency Uncertainties

For this part, the system (3.1) and its estimator (3.7) were integrated on the temporal interval $[0, \frac{10}{75}]$. We used a 1% level of noise in the terms $D\eta_1(t)$ and $E\eta_2(t)$ for all frequency uncertainty studies.

6.1.1 Control design with uncertainties not included in controller design

To demonstrate the effects of frequency uncertainties on the controller performance we chose the exogenous signal

$$F(t) = 2.04 \sin[470(1+\alpha)\pi t] = 2.04 \sin[2\pi(\omega_0(1+\alpha)t)]$$

with nominal component

$$F_0(t) = 2.04 \sin[470\pi t] = 2.04 \sin[2\pi\omega_0 t],$$

where the number α denotes the percentage error in the frequency $(-0.05 \leq \alpha \leq 0.05)$ and $\omega_0 = 235$ Hz denotes the nominal component of the frequency.

(rms) Sound Pressure Level at (ζ,ψ)=(.3,.1) - (dB)				
% freq. error	$\omega_0(1+\alpha)$	Open Loop	Full State	Compensator
-5	223.25	84.7	81.9	81.5
-4	225.60	84.3	81.3	80.4
-3	227.95	83.7	82.6	81.4
-2	230.30	83.3	82.2	81.4
-1	232.65	83.1	76.4	77.3
0	235.00	82.6	70.1	70.3
+1	237.35	82.2	80.5	77.8
+2	239.70	81.9	82.1	79.8
+3	242.05	81.5	80.4	78.7
+4	244.40	81.1	79.0	77.7
+5	246.75	80.8	79.5	77.8

Table 1: *Example 1: Uncertainties not included in design* – Comparison of H^∞ controller with simulated full state feedback, output feedback with compensator, and open loop pressure levels at cavity point $(0.3, 0.1)$ for the time interval $[\frac{3}{75}, \frac{10}{75}]$.

In Table 1, we compared the H^∞ full state feedback controller and the H^∞ compensator with the open loop case for various values of frequency uncertainties in the term $F(t)$. The root mean square (rms) sound pressure level at the point $(0.3, 0.1)$ was used to test the robustness of the controller for these frequencies. It can be observed from Table 1 that for a small error, $\alpha = \pm 1\%$, the H^∞ compensator is comparable to the full state feedback H^∞ controller, with both giving unsatisfactory performance for higher frequency percentage errors.

6.1.2 Control design with uncertainties incorporated

Here the frequency and/or amplitude uncertainties was incorporated in the controller design in an effort to obtain satisfactory performance of the H^∞ compensator in the presence of such uncertainties.

Uncertainties in the frequency: The $\tilde{D}\tilde{\eta}(t)$ term used here is given by equation (5.1). Based on this new uncertainty, we generate the H^∞ compensator. The plant uncertainties now contain both modelling uncertainties and uncertainties in the tracking variable. We consider the same forcing function $F(t)$ as before, namely $F_0(t) = 2.04\sin[2\pi(235t)]$ and $F(t) = 2.04\sin[2\pi(235(1+\alpha)t)]$ where once again α denotes the percentage error in the frequency $(-0.05 \le \alpha \le 0.05)$. We then have (for frequency $\omega_0 = 235$ Hz and amplitude $\beta = 2.04$)

$$\begin{aligned}
F(t) = \beta\sin[2\pi\omega_0(1+\alpha)t] &= \beta\sin[2\pi\omega_0 t] + \beta\left(\sin[2\pi\omega_0(1+\alpha)t] - \sin[2\pi\omega_0 t]\right) \\
&= \beta\sin[2\pi\omega_0 t] + 2\beta\cos\left[2\pi\left(1+\frac{\alpha}{2}\right)\omega_0 t\right]\cdot\sin\left[2\pi\frac{\alpha}{2}t\right] \\
&= F_0(t) + \Delta F(t).
\end{aligned}$$

In Table 2, we present the rms pressure level of the point $(0.3, 0.1)$ for the time interval $[\frac{3}{75}, \frac{10}{75}]$ where a study of the effects of the frequency error was undertaken. In this case, the frequency uncertainty ranges from -2% to 2% thus giving an uncertainty range of about ± 5 Hz. The negative effect of the frequency uncertainties can be seen in both the state controller and the compensator performance where the sound pressure level reaches the open loop pressure levels. A comparison with the results in Table 1 illustrate that the incorporation of the uncertainty in the controller design has not improved the control authority and in some cases, less control is obtained.

(rms) Sound Pressure Level at (ζ,ψ)=(.3,.1) - (dB)				
% error in ω_0	$\omega_0(1+\alpha)$	Open Loop	Full State	Compensator
-2	230.30	83.3	81.1	81.9
-1	232.65	83.1	76.4	77.7
0	235.00	82.6	70.0	70.2
+1	237.35	82.2	80.5	78.4
+2	239.70	81.9	82.1	80.4

Table 2: *Example 1: Uncertainties in frequency considered:* – Comparison of H^∞ controller with simulated full state feedback, output feedback with compensator, and open loop pressure levels at cavity point $(0.3, 0.1)$ for the time interval $[\frac{3}{75}, \frac{10}{75}]$.

Uncertainties in both frequency and amplitude: The forcing function here was taken to be $F_0(t) = 2.04\sin[2\pi\omega_0 t]$, and $F(t) = 2.04(1+\epsilon)\sin[2\pi\omega_0(1+\alpha)t]$ where ϵ denotes the percentage error in the amplitude ($-0.25 \leq \epsilon \leq 0.25$). The term $\tilde{D}\tilde{\eta}(t)$ is again given by (5.1) and in this case we have

$$\begin{aligned} F(t) &= \beta(1+\epsilon)\sin[2\pi\omega_0(1+\alpha)t] \\ &= \beta\sin[2\pi\omega_0 t] + \beta\epsilon\sin[2\pi\omega_0 t] + \beta(1+\epsilon)\left(\sin[2\pi\omega_0(1+\alpha)t] - \sin[2\pi\omega_0 t]\right) \\ &= F_0(t) + \beta\epsilon\sin[2\pi\omega_0 t] + 2\beta(1+\epsilon)\cos\left[2\pi\left(1+\frac{\alpha}{2}\right)\omega_0 t\right]\cdot\sin\left[2\pi\frac{\alpha}{2}t\right] \\ &= F_0(t) + \Delta F(t). \end{aligned}$$

In order to study first the effects of amplitude variations on the controller performance, we kept the uncertainty in the frequency fixed at zero (i.e. $\alpha \equiv 0$) and the uncertainty in the amplitude ranged over $-0.25 \leq \epsilon \leq 0.25$. The resulting sound pressure levels for the open loop, H^∞ full state feedback and H^∞ compensator are summarized in Table 3.

(rms) Sound Pressure Level at (ζ,ψ)=(.3,.1) - (dB), $\alpha = 0.00$				
% ampl. error	$\beta(1+\epsilon)$	Open Loop	Full State	Compensator
-25	1.5300	80.1	71.2	72.8
-10	1.8360	81.6	70.3	71.3
-5	1.9380	82.1	70.1	70.8
-2	1.9992	82.4	70.1	70.4
-1	2.0196	82.5	70.0	70.3
0	2.0400	82.6	70.0	70.2
+1	2.0604	82.6	70.0	70.1
+2	2.0808	82.7	70.0	69.9
+5	2.1420	82.9	70.1	69.6
+10	2.2440	83.4	70.2	68.9
+25	2.5500	84.5	71.1	66.8

Table 3: *Example 1: Uncertainties in amplitude only:* – Comparison of H^∞ controller with simulated full state feedback, output feedback with compensator, and open loop pressure levels at cavity point $(0.3, 0.1)$ for the time interval $[\frac{3}{75}, \frac{10}{75}]$.

Considering first the open loop case, it is noted that increasing values of ϵ lead to monotone increasing rms sound pressure levels in accordance with the monotone increasing levels in the driving force. This is consistent with physical intuition. The rms sound pressure levels in the H^∞ full state feedback and output feedback cases do not exhibit this behavior, however. The former case exhibits optimal reduction when no noise is present in the force whereas the latter exhibits monotone decreasing sound pressure levels as ϵ is increased. Finally, we found that the rms levels of the controlling voltages in *both* cases decrease monotonically as ϵ is increased as depicted in Table 3b below.

(rms) Input Voltage - (volts), $\alpha = 0.00$			
% ampl. error	$\beta(1+\epsilon)$	Full State	Compensator
-25	1.5300	28.44	27.09
-10	1.8360	27.62	27.05
-5	1.9380	27.32	27.04
-2	1.9992	27.15	27.03
-1	2.0196	27.08	27.03
0	2.0400	27.02	27.02
+1	2.0604	26.96	27.02
+2	2.0808	26.90	27.02
+5	2.1420	26.71	27.01
+10	2.2440	26.39	26.99
+25	2.5500	25.35	26.96

Table 3b: *Example 1: Uncertainties in amplitude only:* – Comparison of H^∞ controller with simulated full state feedback and output feedback with compensator rms voltage for the time interval $[\frac{3}{75}, \frac{10}{75}]$.

This difference in behavior between the full state and output feedback cases provides some insight into the manner through which the tracking variable $r(t)$ contributes to the controlling voltage in the case of exogenous input. We recall that the controlling voltages in the full state and output feedback cases are given by

$$u(t) = -R^{-1}B^T\left[\Pi y(t) - r(t)\right] \quad \text{and} \quad u(t) = -R^{-1}B^T\left[\Pi y_c(t) - r(t)\right] \ ,$$

respectively.

The state y, modeling the actual process, is driven by the error-contaminated force. The tracking variable r, on the other hand, is generated using the measured, nominal component to the force. The previously discussed H^∞ full state feedback control results depend upon y and r being balanced in the sense that they are generated by the same forcing function (in the form F and ΠF, respectively). Deviation from this balance by adding either positive or negative error to the amplitude leads to degradation of control authority as noted in the full state feedback column of Table 3. In this example, the inconsistency between the measured force driving r and the actual force driving y leads to higher sound pressure levels when either positive and negative amplitude errors are present.

In the case of output feedback, the state estimator y_c and tracking variable r are both generated using the nominal amplitude of the force. Hence the uncertainties arise only in the magnitude of the observed state y_{ob} (see (3.7)). For this example, the balance between the state equation (3.1), which models the physical process, the form of the observation (3.10) and the state estimator (3.7) is such that increasing force amplitude levels lead to increased control penalties which in turn yield monotonically improving controlled sound pressure levels.

This illustrates that the behavior of the H^∞ full state and output feedback controllers can differ significantly in the presence of noise in the data. It also illustrates that reasonable control can be obtained with relatively significant uncertainty levels in the amplitude of the driving signal.

Continuing in the same spirit as above, we now set the frequency uncertainty level at 1% (i.e. $\alpha = +0.01$, new plant frequency $= (1.01)\omega_0 \equiv 237.35$ Hz) and vary the amplitude uncertainty, ϵ, between $-0.25 \leq \epsilon \leq 0.25$. The effects of frequency and amplitude uncertainties on the performance of the H^∞ controllers (measured via the sound pressure levels of the cavity point $(0.3, 0.1)$) are illustrated in Table 4.

(rms) Sound Pressure Level at (ζ, ψ)=(.3,.1) - (dB), $\alpha = +0.01$				
% ampl. error	$\beta(1+\epsilon)$	Open Loop	Full State	Compensator
-25	1.5300	79.7	79.6	78.1
-10	1.8360	81.3	80.2	78.2
-5	1.9380	81.7	80.4	78.3
-2	1.9992	81.9	80.5	78.3
-1	2.0196	82.1	80.5	78.4
0	2.0400	82.2	80.5	78.4
+1	2.0604	82.2	80.6	78.4
+2	2.0808	82.3	80.6	78.4
+5	2.1420	82.6	80.7	78.5
+10	2.2440	83.0	80.9	78.5
+25	2.5500	84.1	81.5	78.8

Table 4: *Example 1: Uncertainties in both frequency and amplitude:–* Comparison of H^∞ controller with simulated full state feedback, output feedback with compensator, and open loop pressure levels at cavity point $(0.3, 0.1)$ for the time interval $[\frac{3}{75}, \frac{10}{75}]$.

A direct comparison of Tables 3 and 4 reveals that amplitude uncertainties can be tolerated whereas frequency uncertainties can be dentrimental to the closed loop performance. The H^∞ control methodology provides a robustness in performance with respect to amplitude uncertainties and in some cases, the output feedback case can even outperform the full state controller. This is not only attractive from an implementational point of view, as it is seldom the case that full state is available, but performancewise, the output feedback case can, in some cases provide better results. In the presence of frequency uncertainties, however, neither the H^∞ full state feedback or the H^∞ compensator provided adequate robustness and controlled sound pressure levels only slightly below those in the open loop case were obtained. While robustness with respect to frequency uncertainties is a difficult goal, it is physically important since variations and uncertainties in frequency commonly arise in applications. Hence further work toward robustness in this aspect is needed.

6.2 Example 2: Time Delays

In this section we will consider the effects of time delays in the input voltage $u(t)$, the measured output $y_{ob}(t)$, and the forcing function $F(t)$. The delayed input and forcing function enter the plant state equation (3.1) and the delayed output enters the estimator equation (3.7). The discrete time approximations of the above signals are given below.

Discrete Time Approximations:

(i) Plant state, $y(t) = y_k$ for $t \in [t_k, t_k + \Delta t_k)$

(ii) Estimator state, $y_c(t) = y_{c_k}$ for $t \in [t_k, t_k + \Delta t_k)$

(iii) Plant output, $y_{ob}(t) = y_{ob_k}$, for $t \in [t_k, t_k + \Delta t_k)$

(iv) Input voltage, $u(t) = u_k$ for $t \in [t_k, t_k + \Delta t_k)$

(v) Forcing function, $F(t) = F_k$ for $t \in [t_k, t_k + \Delta t_k)$

Delayed Signals:

(i) Plant output, $y_{ob}(t) = y_{ob}(t - m_o\Delta t) = y_{ob_{k-m_o}}$ for $t \in [t_k, t_k + \Delta t_k)$

(ii) Input voltage, $u(t) = u(t - m_i\Delta t) = u_{k-m_i}$ for $t \in [t_k, t_k + \Delta t_k)$

(iii) Forcing function (plant only), $F(t) = F(t - m_f\Delta t) = F_{k-m_f}$ for $t \in [t_k, t_k + \Delta t_k)$.

Then, the plant and estimator state equations with delays can be formulated as follows

State with Delayed Input Voltage and/or Forcing:

$$\dot{y}(t) = Ay(t) + Bu_{k-m_i} + \tilde{D}\tilde{\eta}(t) + F_{k-m_f}, \tag{6.1}$$

Estimator with Delayed Output:

$$\dot{y}_c(t) = A_c y_c(t) + [BR^{-1}B^T - \frac{1}{\gamma^2}\tilde{D}\tilde{D}^T]r(t) + F_c y_{ob_{k-m_o}} + F(t). \tag{6.2}$$

The driving frequency for this example was taken to be 235 Hz and the data was assumed to be sampled at 3750 Hz; therefore for each time delay Δt_k we have a

$$360^o \times \frac{235\,Hz}{3750\,Hz} = 22.56^o$$

delay in the signals.

In the simulations, the exact values of phase shifts were approximated since we used integer multiples of the time step Δt for the delays. For example, we approximated 360^o with 16 delays $\approx 360.96^o$; further correspondence of the implemented and actual delay is summarized in Table 5 below.

Implemented Delay (approximated)	Actual Delay
360^o+1 delays = 17 delays = 383.52^o	360^o+1 delays = 382.56^o
360^o+2 delays = 18 delays = 406.08^o	360^o+2 delays = 405.12^o
360^o−1 delays = 16 delays = 338.40^o	360^o−1 delays = 337.44^o
360^o−1/2 delays = 15.5 delays = 349.68^o	360^o−1/2 delays = 348.72^o
360^o+1/2 delays = 16.5 delays = 372.24^o	360^o+1/2 delays = 371.28^o

Table 5: *Example 2:–* Correspondence of implemented and actual delays.

Table 6a illustrates the effects of time delays on the performance of the H^∞ output feedback controller. First, a number of simulations involving integer and fractional values of time delays in the forcing function were performed to test the performance of the compensator. As illustrated by the first set of results in the table, good attenuation is obtained even with significant delays in the force. The effect of discrete time approximation can also be seen in the case of 360^o delays. Unfortunately, such positive results were not observed in the case of time delays in the input signal $u(t)$. Even in the case of one third of a time delay, which corresponds to about 7.5^o, unacceptable results that parallel those of the open loop case were obtained. Slightly more acceptable results were obtained for the case of small time delays in the output signal $y_{ob}(t)$, where for half a time delay, the compensator was able to provide acceptable pressure levels. However, for larger delays, unacceptable results were obtained here also.

(rms) Sound Pressure Level at (ζ,ψ)=(.3,.1) - (dB)			
Output Delays	Input voltage	Forcing function	Pressure
0^o	0^o	0^o	70.0
Delays in forcing function $F(t)$			
0^o	0^o	0^o+1 delay	70.8
0^o	0^o	0^o+2 delays	74.0
0^o	0^o	0^o+3 delays	76.8
0^o	0^o	0^o+4 delays	78.8
0^o	0^o	360^o-1 delay	72.8
0^o	0^o	360^o+0 delays	69.9
0^o	0^o	360^o+1 delay	70.9
0^o	0^o	360^o+2 delays	74.2
Delays in output $y_{ob}(t)$			
0^o+1/2 delay	0^o	0^o	69.2
0^o+1/2 delay	0^o	0^o+1/2 delay	69.2
0^o+1 delay	0^o	0^o	108.4
$360^o-1/2$ delay	0^o	0^o	unbdd
360^o+1/2 delay	0^o	0^o	unbdd
Delays in input $u(t)$			
0^o	0^o+1/3 delay	0^o	83.3
0^o	0^o+1/2 delay	0^o	83.7
0^o	0^o+1 delay	0^o	unbdd
0^o	0^o+1/2 delay	0^o+1/2 delay	83.7
0^o	0^o+1/2 delay	360^o+1/2 delay	83.8
0^o	0^o+1/2 delay	$360^o-1/2$ delay	82.7

Table 6a: Effects of time delays in forcing function, input and output signals on the H^∞ compensator performance for the time interval $[\frac{3}{75},\frac{30}{75}]$. Results on simulated cavity pressure at point $(0.3, 0.1)$ where the open loop pressure level is 82.6dB. Note that 1 delay $\approx 22.56^o$.

In the last case of Table 6a concerning delays in the voltage input $u(t)$, we made an additional study regarding the delay contributions of the components of the input voltage. To do so, we isolated the contributions from the estimator state $y_{c_{k-m_e}}$ and the tracking signal r_{k-m_t}, which are

$$u(t) = -R^{-1}B^T[\Pi y_{c_{k-m_e}} - r(t)],$$
$$u(t) = -R^{-1}B^T[\Pi y_c(t) - r_{k-m_t}],$$

respectively. This was done to see if the performance degradation is due to delays in the state $y_c(t)$ or due to delays in the tracking variable $r(t)$. The delays in the signal $r(t)$ were actually introduced by delays in the exogenous signal $F(t)$ via (3.5). In Table 6b below we compare these findings with the case of no delay in the voltage input.

Delays	Input voltage u(t)	Pressure (dB)
no delays in u	$-Ky_c(t)+R^{-1}B^Tr(t)$	70.0
1/2 delay in u	$-Ky_{c_{k-\frac{1}{2}}}+R^{-1}B^Tr_{k-\frac{1}{2}}$	83.7
1/2 delay in y_c	$-Ky_{c_{k-\frac{1}{2}}}+R^{-1}B^Tr(t)$	79.4
1/2 delay in r	$-Ky_c(t)+R^{-1}B^Tr_{k-\frac{1}{2}}$	76.7

Table 6b: Contributions of the time delays on the components of u(t) for the interval $[\frac{3}{75},\frac{30}{75}]$. Results on simulated cavity pressure at $(0.3, 0.1)$.

From this set of simulations we can observe that the performance degradation due to delays in the voltage input can be substantial whether the delay is in the estimator or the tracking variable. Even though delay in y_c appears to be more serious than delay in r, both contribute to substantial degradation of performance. From the results in Tables 6a and 6b, we see that for this system, the H^∞ theory provides little robustness in the presence of certain types of delays. From the perspective of implementation, this issue is crucial since hardware delays and phase shifts due to filters, A/D and D/A conversions, et cetera, are unavoidable in any system. As indicated by numerical and experimental results in [15], this issue can be partially resolved in some systems by performing a "delay identification" of the system before implementing control. For more complex coupled systems such as that considered here, however, such identification techniques will become difficult, thus necessitating the development of control results which have additional robustness with respect to delays and phase shifts.

6.3 Example 3: $\mathbf{H^\infty}$ vs LQG

In this example, some of the effects of γ on the overall performance of the closed loop system and on the numerical implementation of the finite dimensional H^∞ compensator for this system are examined. As a test, we varied the value of γ and compared the condition numbers of the two Riccati solutions. These results along with corresponding sound pressure levels at the point $(0.3, 0.1)$ are summarized in Table 7.

As noted in the last column of the table, the sound pressure level remains relatively unchanged as $\gamma \to \infty$. Hence when this is used as a measure for comparison of the two methodologies, little significant differences can be noted for this system. The condition numbers of both Riccati solutions appear to be rather insensitive to increasing γ. Hence from a numerical point of view the Kalman filter is computationally more attractive when applied to this system as the Riccati equations have a simpler form.

Effects of γ				
γ^2	cond(Π)	cond(Σ)	$\rho(\Pi\Sigma)$	Pressure (dB)
2.89	2.740×10^{18}	2.044×10^{17}	0.659	70.0159
5.00	9.759×10^{19}	2.041×10^{17}	21.749	70.0142
10.00	2.404×10^{16}	2.038×10^{17}	0.353	70.0131
20.00	1.152×10^{18}	2.037×10^{17}	8.688	70.0125
50.00	9.467×10^{24}	2.037×10^{17}	561.367	70.0950
100.00	2.401×10^{16}	2.037×10^{17}	0.934	70.0121
500.00	1.694×10^{16}	2.036×10^{17}	1.810	70.0120
1000.00	2.517×10^{16}	2.036×10^{17}	2.540	70.0120
5000.00	2.415×10^{16}	2.036×10^{17}	5.578	70.0120
10000.00	2.672×10^{16}	2.036×10^{17}	7.898	70.0120
∞	2.062×10^{16}	2.036×10^{17}	12.801	70.0120

Table 7: *Example 3 :* – Comparison of H^∞ and LQG compensators. Effects on condition numbers and pressure levels at cavity point $(0.3, 0.1)$.

6.4 Example 4: Effects of $r(t)$

Since the tracking variable must be integrated backward in time before calculating the input voltage

$$u(t) = -Ky_c(t) + R^{-1}B^T r(t),$$

a natural idea would be to remove this signal since it consumes computational time and requires complete knowledge of the exogenous force. In this case the signal would be given by

$$u(t) = -Ky_c(t). \tag{6.3}$$

In this case, possible state estimators with the control law (6.3) are

Case I $$\dot{y}_c(t) = \left[A - F_cC - BK + \frac{1}{\gamma^2}DD^T\Pi\right] y_c(t) + F_c y_{ob}(t),$$

or

Case II $$\dot{y}_c(t) = \left[A - F_cC - BK + \frac{1}{\gamma^2}DD^T\Pi\right] y_c(t) + F_c y_{ob}(t) + F(t).$$

In Case I we assume that no information regarding $F(t)$ is available whereas in Case II we assume that the exogenous input $F(t)$ is known and used in the state estimator.

A significant saving in computational time would result by excluding the backward (in time) integration of $r(t)$ at the expense of a controller with less authority. In the results presented below, we used four different frequencies that excite primarily either beam and/or cavity modes. The Riccati solutions to (3.4) and (3.8) were generated with a value of $\gamma = 1.00$.

In Table 8 below we summarize typical results. The effects of each frequency on the (rms) voltage and the (rms) sound pressure level (SPL) at the point $(0.3, 0.1)$ are presented. The open loop, full state feedback and full state feedback without tracking variable are included for comparison to the results for the compensator with tracking signal and Cases I and II.

For all these simulations, a 1% disturbance level in the terms $D\eta_1(t)$ and $E\eta_2(t)$ was used. The four forcing functions used were

(a) Off-Resonant Excitation:

$$f(t,\zeta) = 2.04\sin(470\pi t)$$

(b) Multiple Resonant Excitation I:

$$f(t,\zeta) = 2.04[\sin(150\pi t) + \sin(790\pi t)]$$

(c) Multiple Resonant Excitation II:

$$f(t,\zeta) = 2.04[\sin(150\pi t) + \sin(320\pi t) + \sin(454\pi t) + \sin(603\pi t)]$$

(d) Cavity Excitation:

$$f(t,\zeta) = 2.04\sin(650\pi t)$$

	(a) off-res.		(b) mult. res. I		(c) mult. res. II		(d) cavity	
input voltage	rms volt	SPL @ (.3,.1)	rms volt	SPL @ (.3,.1)	rms volt	SPL @ (.3,.1)	rms volt	SPL @ (.3,.1)
open loop	0	82.2	0	98.4	0	96.6	0	81.4
$-Ky_c(t) + R^{-1}B^T r(t)$	22.3	70.0	59.8	83.7	47.7	77.5	40.0	77.9
$-Ky_c(t)$ (I)	2.5	72.9	10.9	97.1	13.9	95.7	0.6	80.1
$-Ky_c(t)$ (II)	16.0	76.9	13.4	89.7	24.4	89.2	3.7	82.2
$-Ky(t) + R^{-1}B^T r(t)$	22.3	69.9	59.8	83.7	47.7	77.5	40.0	77.9
$-Ky(t)$	16.0	76.9	13.4	89.7	24.4	89.2	3.7	82.2

Table 8: *Example 4 :* – Effects of various frequencies on the simulated rms voltage and cavity pressure at point $(0.3, 0.1)$ for open loop, H^∞ full state controller with and without r(t) and for the H^∞ compensator with r(t) and Cases I, II.

Below, we discuss, in regard to Table 8, the effects of each frequency on the controller performance. Furthermore, we provide additional results of the sound pressure levels at five cavity points, rms displacement and/or velocity at five beam points, and voltage plots with discussions regarding each individual frequency used.

(a) Off-Resonant Excitation: This frequency of 235Hz is approximately halfway between the natural frequencies of the first and fourth mode, see [5, 9]. Case I outperforms Case II by about 4dB, but neither surpass the compensator with the tracking signal included, as seen in Table 8. The (rms) voltage used in Case I is about a tenth of the voltage used in the ideal case (H^∞ compensator with tracking signal). The corresponding voltage for Case II is about two thirds of the corresponding one for the ideal case and is exactly the same as the H^∞ full state controller without $r(t)$.

The pressure levels of five additional cavity points are presented in Table 9a for this frequency. For these points, Case I gives somewhat better results than Case II, with an average of 1dB difference in pressure levels. In some points we can see that both Case I and II perform worse than the open loop case. Once again, the compensator performance (ideal case) can be seen to surpass both Cases by at least 13dB.

input voltage	rms voltage	Pressure Level (dB) at cavity point:					
		(.3,.1)	(.1,.5)	(.5,.5)	(.3,.2)	(.3,.5)	(.3,.8)
open loop	0	82.2	71.4	71.4	82.6	71.2	83.4
$-Ky_c(t) + R^{-1}B^T r(t)$	22.3	70.0	55.2	55.2	65.2	56.3	63.1
$-Ky_c(t)$ (I)	2.5	72.9	72.7	72.7	78.7	72.6	80.9
$-Ky_c(t)$ (II)	16.0	76.9	73.9	73.9	80.4	73.9	82.1
$-Ky(t) + R^{-1}B^T r(t)$	22.3	69.9	53.9	53.9	65.1	54.7	62.8
$-Ky(t)$	16.0	76.9	73.9	73.9	80.4	73.8	82.1

Table 9a : *Example 4 - Off Resonance Excitation :* – Effects on the simulated rms voltage and cavity pressure at 5 points for open loop, H^∞ full state controller with and without r(t) and for the H^∞ compensator with r(t) and Cases I, II. Results for the time interval $[\frac{3}{75}, \frac{30}{75}]$, with $\gamma^2 = 1$.

The (rms) displacement of five points along the beam is presented in Table 9b, where both Cases are compared to the ideal case. For some points, specifically at 0.12 and at 0.48, the rms displacement for Case I is lower than that of Case II, which (Case II) is larger than the open loop case. It is also worth noticing that at these points, the rms displacement is lower than the ideal case. In the rest of the beam points, i.e. at 0.24, 0.30 and 0.36, we observe that the reverse occurs; that is Case II has lower rms displacement than that of Case I, with both Cases performing better than the open loop case but with both exceeding that of the ideal case.

input voltage	rms displacement ($\times 10^{-7}$) at :				
	0.12	0.24	0.30	0.36	0.48
open loop	6.2	16.0	17.7	16.0	6.2
$-Ky_c(t) + R^{-1}B^T r(t)$	4.4	4.2	5.4	4.2	4.4
$-Ky_c(t)$ (I)	2.2	7.9	9.2	7.9	2.2
$-Ky_c(t)$ (II)	6.4	6.9	8.1	6.9	6.4
$-Ky(t) + R^{-1}B^T r(t)$	4.4	4.3	5.4	4.3	4.4
$-Ky(t)$	6.4	7.0	8.1	7.0	6.4

Table 9b : *Example 4 - Off Resonance Excitation :* – Effects on the simulated rms displacement at 5 beam points for open loop, H^∞ full state controller with and without r(t) and for the H^∞ compensator with r(t) and Cases I, II. Results for the time interval $[\frac{3}{75}, \frac{30}{75}]$, with $\gamma^2 = 1$.

Continuing with the effects of this frequency, we duplicated the results of Table 9a for a value of $\gamma^2 = 10,000 \approx \infty$ and presented them in Table 9c. This, in essence, compares the standard LQG/Kalman filter with the H^∞/MinMax control methodology. Identical results were obtained for the rms voltages and no significant differences were observed for the pressure levels at all six cavity points.

input voltage	rms voltage	Pressure Level (dB) at cavity point:					
		(.3,.1)	(.1,.5)	(.5,.5)	(.3,.2)	(.3,.5)	(.3,.8)
open loop	0	82.2	71.4	71.4	82.5	71.2	83.4
$-Ky_c(t) - R^{-1}B^Tr(t)$	22.3	70.0	55.2	55.2	65.2	56.3	63.0
$-Ky_c(t)$ (I)	2.5	72.9	72.7	72.7	78.6	72.5	80.9
$-Ky_c(t)$ (II)	16.0	76.9	73.9	73.9	80.4	73.9	82.1
$-Ky(t) - R^{-1}B^Tr(t)$	22.3	70.0	53.9	53.9	65.0	54.7	62.8
$-Ky_c(t)$	16.0	76.9	73.9	73.9	80.4	73.8	82.1

Table 9c: *Example 4 - Off Resonance Excitation :* – Effects on the simulated rms voltage and cavity pressure at 5 points for open loop, H^∞ full state controller with and without r(t) and for the H^∞ compensator with r(t) and Cases I, II. Results for the time interval $[\frac{3}{75}, \frac{30}{75}]$, with $\gamma^2 = 10,000$.

(b) Multiple Resonant Excitation I: This frequency excites the first and fourth modes, [9]. The reverse effect on the pressure level is observed (in Table 8) in this choice of frequency; Case II outperforms Case I by 7dB with Case I approaching the open loop performance. It is worth noting that the attenuation levels in Case I and Case II were obtained with roughly 1/5 the voltage used in the ideal case.

input voltage	rms voltage	Pressure Level (dB) at cavity point:					
		(.3,.1)	(.1,.5)	(.5,.5)	(.3,.2)	(.3,.5)	(.3,.8)
open loop	0	98.4	92.8	92.8	95.0	92.5	90.2
$-Ky_c(t) + R^{-1}B^Tr(t)$	59.9	83.7	68.2	68.2	77.5	65.7	63.0
$-Ky_c(t)$ (I)	11.0	97.1	91.3	91.3	93.7	91.1	89.2
$-Ky_c(t)$ (II)	13.5	89.7	83.7	83.7	86.0	83.6	81.3
$-Ky(t) + R^{-1}B^Tr(t)$	59.9	83.7	68.1	68.1	77.5	65.5	62.8
$-Ky(t)$	13.5	89.7	83.7	83.7	86.1	83.6	81.3

Table 10a : *Example 4 - Multiple Resonance Excitation I :* – Effects on the simulated rms voltage and cavity pressure at 5 points for open loop, H^∞ full state controller with and without r(t) and for the H^∞ compensator with r(t) and Cases I,II. Results for the time interval $[\frac{3}{75}, \frac{30}{75}]$, with $\gamma^2 = 1$.

The pressure levels of the other five cavity points exhibit identical behavior to that of the point (.3, .1) as observed in Table 10a; that is, Case II outperforms Case I *and* both have lower rms pressure levels than the open loop case. In some points though, Case I has rms pressure levels close to the open loop case. This can also be observed at the rms displacement of five beam points where both cases perform somewhere between the open loop and the ideal case, with Case II performing (smaller rms displacement) better than Case I, see, Table 10b.

input	rms displacement ($\times 10^{-7}$) at point:				
voltage	0.12	0.24	0.30	0.36	0.48
open loop	116.2	267.9	292.8	267.9	116.2
$-Ky_c(t) + R^{-1}BTr(t)$	7.3	10.8	15.0	10.8	7.3
$-Ky_c(t)$ (I)	90.9	207.0	226.5	207.0	90.9
$-Ky_c(t)$ (II)	34.8	85.7	94.0	85.7	34.8
$-Ky(t) + R^{-1}B^T r(t)$	7.3	10.9	15.0	10.9	7.3
$-Ky(t)$	34.9	85.8	94.1	85.8	34.9

Table 10b : *Example 4 - Multiple Resonance Excitation I :* – Effects on the simulated rms displacement at 5 beam points for open loop, H^∞ full state controller with and without r(t) and for the H^∞ compensator with r(t) and Cases I,II. Results for the time interval $[\frac{3}{75}, \frac{30}{75}]$, with $\gamma^2 = 1$.

In addition to the rms voltages (on the time interval $[\frac{3}{75}, \frac{30}{75}]$), we also looked at the corresponding time plots of these voltages, as depicted in Figure 4. First, both the H^∞ compensator (plot 4(a)) and the H^∞ state controller (plot 4(d)) do not exceed ± 100 volts, which is resonable for piezoceramic patches of this size, see, [9, 12]. Both voltages of Case I, and II (plots 4(b) and 4(c)) are much smaller compared to the one for the ideal case. In fact, it can be observed that both voltages (plots 4(b) and 4(c)), and even plot 4(e) for the H^∞ full state without the signal $r(t)$, are indeed about one fifth of the voltage used in the ideal case, as mentioned above for the (rms) voltage levels.

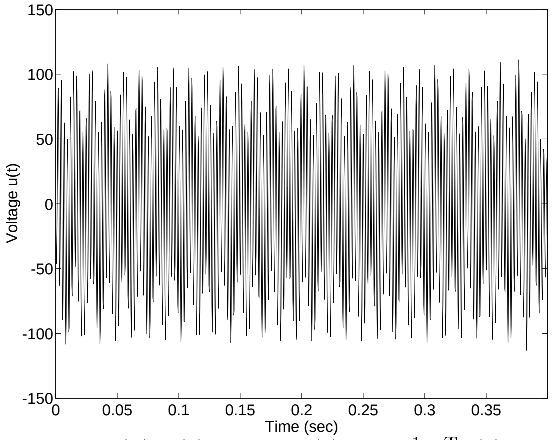

(a) $u(t) = -Ky_c(t) + R^{-1}B^T r(t)$

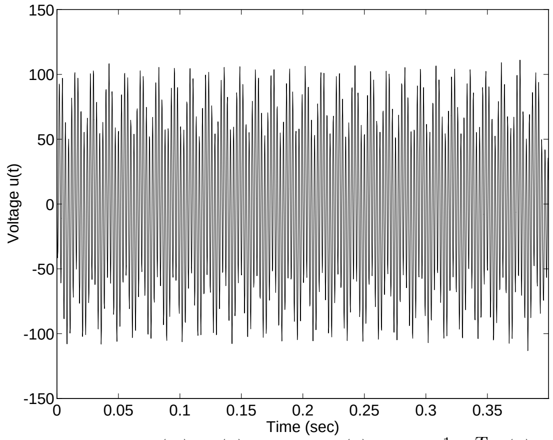

(d) $u(t) = -Ky(t) + R^{-1}B^T r(t)$

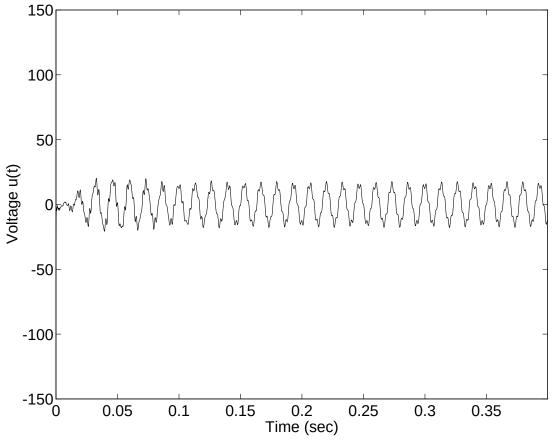

(b) $u(t) = -Ky_c(t)$ (I)

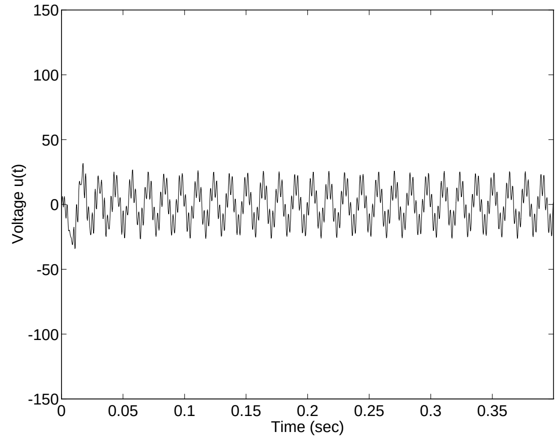

(e) $u(t) = -Ky(t)$

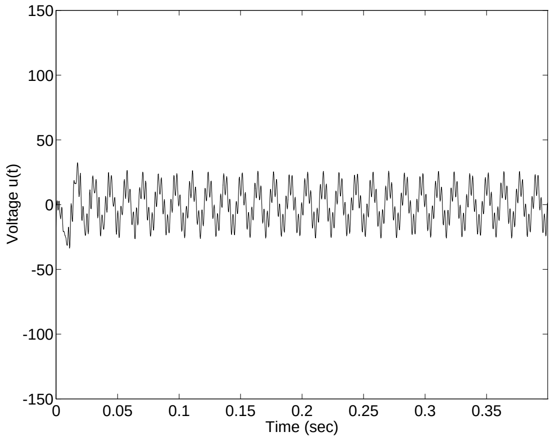

(c) $u(t) = -Ky_c(t)$ (II)

Figure 4: *Example 4 - Multiple Resonant Excitation I :* Effects on the simulated voltage for H^∞ full state controller with and without $r(t)$ and for the H^∞ compensator with $r(t)$ and Cases I, II. Results for the time interval $[0, 0.4]$.

(c) Mupliple Resonant Excitation II: Both cases (I & II) perform poorly and in some cavity points they perform worse than the open loop case as seen on Table 11a. For some cavity points Case I gives somewhat better pressure levels than Case II and for some other, the reverse is observed. This is not the case though for the rms displacement and rms velocity, as depicted in Tables 11b and 11c, respectively, where Case II always outperfoms Case I with both having values between the open loop and ideal case. Both cases maintain a small (rms) input voltage compared to the one for the ideal case.

input voltage	rms voltage	Pressure Level (dB) at cavity point:					
		(.3,.1)	(.1,.5)	(.5,.5)	(.3,.2)	(.3,.5)	(.3,.8)
open loop	0	96.6	81.0	81.0	93.2	80.9	92.6
$-Ky_c(t) + R^{-1}B^T r(t)$	47.7	77.5	69.6	69.6	71.4	69.6	71.0
$-Ky_c(t)$ (I)	13.9	95.7	80.4	80.4	92.6	80.3	92.3
$-Ky_c(t)$ (II)	24.4	89.2	82.7	82.7	86.7	82.6	87.4
$-Ky(t) + R^{-1}B^T r(t)$	47.7	77.5	69.6	69.6	71.3	69.5	71.0
$-Ky(t)$	24.4	89.2	82.7	82.7	86.7	82.6	87.4

Table 11a : *Example 4 - Multiple Resonance Excitation II :* – Effects on the simulated rms voltage and cavity pressure at 5 points for open loop, H^∞ full state controller with and without r(t) and for the H^∞ compensator with r(t) and Cases I, II. Results for the time interval $[\frac{3}{75}, \frac{30}{75}]$, with $\gamma^2 = 1$.

input voltage	rms displacement ($\times 10^{-7}$) at point:				
	0.12	0.24	0.30	0.36	0.48
open loop	127.8	300.4	327.8	300.4	127.8
$-Ky_c(t) + R^{-1}B^T r(t)$	7.2	11.7	13.7	11.7	7.2
$-Ky_c(t)$ (I)	89.4	208.3	227.5	208.3	89.4
$-Ky_c(t)$ (II)	34.5	86.3	94.3	86.3	34.5
$-Ky(t) + R^{-1}B^T r(t)$	7.2	11.8	13.9	11.8	7.2
$-Ky(t)$	34.6	86.4	94.5	86.4	34.6

Table 11b : *Example 4 - Multiple Resonance Excitation II :* – Effects on the simulated rms displacement at 5 points for open loop, H^∞ full state controller with and without r(t) and for the H^∞ compensator with r(t) and Cases I, II. Results for the time interval $[\frac{3}{75}, \frac{30}{75}]$, with $\gamma^2 = 1$.

input voltage	rms velocity ($\times 10^{-4}$) at point:				
	0.12	0.24	0.30	0.36	0.48
open loop	55.7	131.4	143.7	131.4	55.7
$-Ky_c(t) + R^{-1}BTr(t)$	9.4	10.9	16.4	10.9	9.4
$-Ky_c(t)$ (I)	42.40	99.1	108.6	99.1	42.4
$-Ky_c(t)$ (II)	19.3	42.7	47.0	42.7	19.3
$-Ky(t) + R^{-1}B^T r(t)$	9.4	10.9	16.4	10.9	9.4
$-Ky(t)$	19.3	42.7	47.0	42.7	19.3

Table 11c : *Example 4 - Multiple Resonance Excitation II :* – Effects on the simulated rms velocity at 5 points for open loop, H^∞ full state controller with and without r(t) and for the H^∞ compensator with r(t) and Cases I, II. Results for the time interval $[\frac{3}{75}, \frac{30}{75}]$, with $\gamma^2 = 1$.

The cavity pressure at the time instant $T = \frac{10}{75}$ sec for all six different types of input voltage is presented in Figure 5. It can be observed from these plots that the cavity pressure for Case I is somewhat between the open loop case and the output feedback case. The similarity between Case II and that of the full state without $r(t)$ is rather striking.

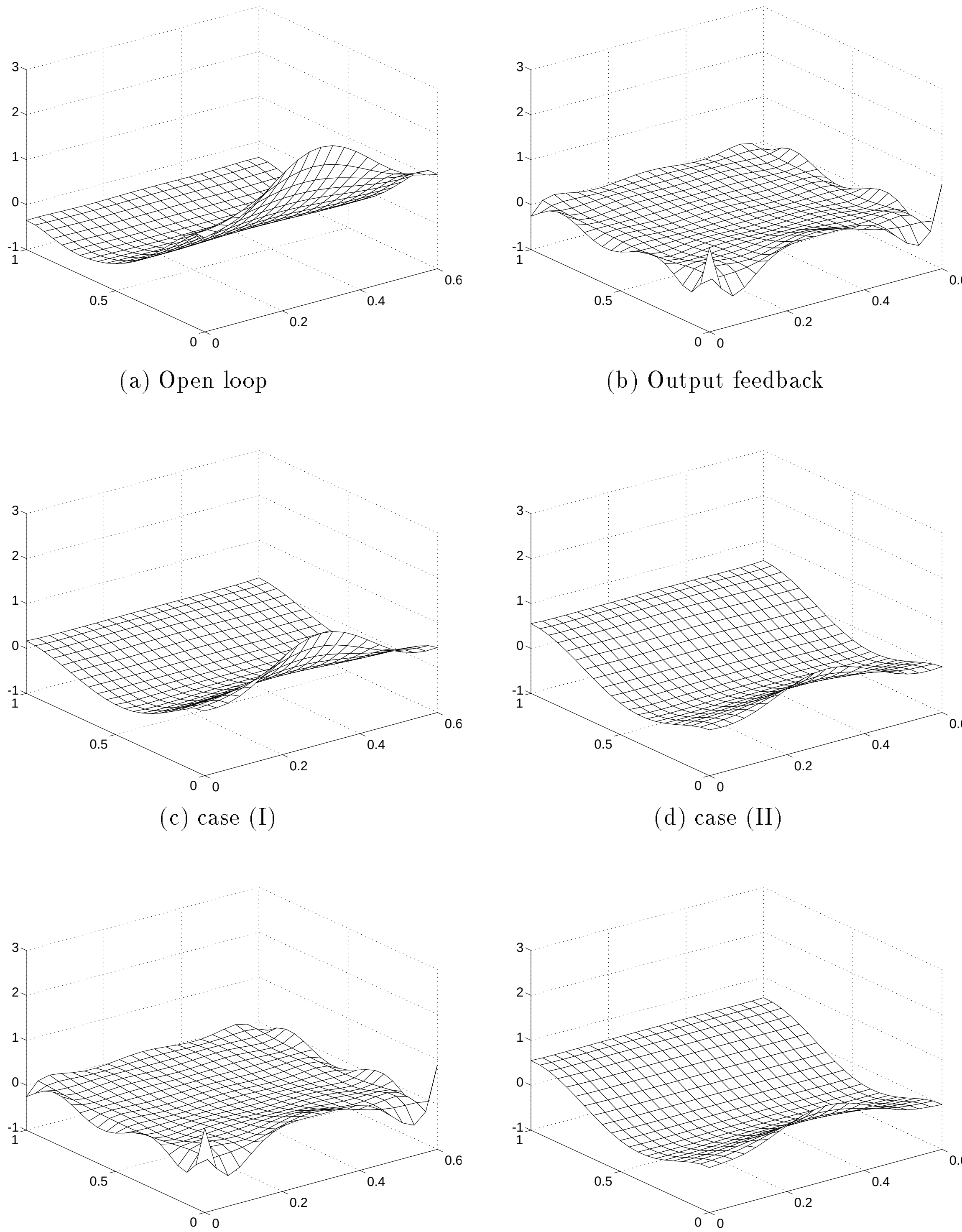

(a) Open loop

(b) Output feedback

(c) case (I)

(d) case (II)

(e) full state with r(t)

(f) full state w/o r(t)

Figure 5: *Example 4:* – Multiple resonant excitation II, cavity pressure at $t = \frac{10}{75}$ sec.

(d) **Cavity Excitation:** The results of this frequency duplicate those for the off-resonant excitation case (part (a) of this example), namely Case I outperforms Case II by almost 2dB. The performance of Case II is worse than the open loop case but by observing the (rms) voltage (an infinitesimal fraction of the output feedback case voltage) used for this scheme, we must not expect much performance from such a controller. A more carefull inspection of the other five cavity points, presented in Table 12a, reveals that for some points, namely (.1, .5), (.5, .5), and (.3, .5), both perform worse than the open loop case.

input	rms	Pressure Level (dB) at cavity point:					
voltage	voltage	(.3,.1)	(.1,.5)	(.5,.5)	(.3,.2)	(.3,.5)	(.3,.8)
open loop	0	81.4	79.5	79.5	74.8	79.3	76.3
$-Ky_c(t) + R^{-1}B^T r(t)$	40.0	77.9	71.6	71.6	67.3	71.3	64.6
$-Ky_c(t)$ (I)	0.6	80.7	80.0	80.0	68.3	79.9	73.4
$-Ky_c(t)$ (II)	3.7	82.2	83.3	83.3	68.9	83.3	76.6
$-Ky(t) + R^{-1}B^T r(t)$	40.0	77.9	71.6	71.6	67.2	71.3	64.4
$-Ky(t)$	3.7	82.2	83.3	83.3	68.8	83.3	76.6

Table 12a : *Example 4 - Cavity Excitation :* – Effects on the simulated rms voltage and cavity pressure at 5 points for open loop, H^∞ full state controller with and without r(t) and for the H^∞ compensator with r(t) and Cases I, II. Results for the time interval $[\frac{3}{75}, \frac{30}{75}]$, with $\gamma^2 = 1$.

The rms displacement levels of both Case I and II, are given below in Table 12b. Both cases have lower levels than the ideal case but we observe that for some points, Case I has lower (than the ideal case) rms displacement levels while for some others the opposite is observed.

input	rms displacement ($\times 10^{-7}$) at point:				
voltage	0.12	0.24	0.30	0.36	0.48
open loop	4.6	10.5	12.1	10.5	4.6
$-Ky_c(t) + R^{-1}B^T r(t)$	3.8	4.6	6.8	4.6	3.8
$-Ky_c(t)$ (I)	1.7	4.0	5.6	4.0	1.7
$-Ky_c(t)$ (II)	2.3	3.8	5.3	3.8	2.3
$-Ky(t) + R^{-1}B^T r(t)$	3.8	4.6	6.9	4.6	3.8
$-Ky(t)$	2.4	3.9	5.4	3.9	2.4

Table 12b : *Example 4 - Cavity Excitation :* – Effects on the simulated rms displacement at 5 beam points for open loop, H^∞ full state controller with and without r(t) and for the H^∞ compensator with r(t) and Cases I, II. Results for the time interval $[\frac{3}{75}, \frac{30}{75}]$, with $\gamma^2 = 1$.

Such a result is not exhibited by the rms velocity, appearing in Table 12c, where the rms velocity levels depend on the location of these points. A closer look at the voltage plots depicted in Figure 6, justifies, in some way, this behavior. The rms displacement and velocity are often lower than those for the ideal case and this might be attributed to the small voltage amplitudes corresponding to Case I (plot 6(b)) and Case II (plot 6(c)).

input	rms velocity ($\times 10^{-4}$) at point:				
voltage	0.12	0.24	0.30	0.36	0.48
open loop	4.2	8.9	12.2	8.9	4.2
$-Ky_c(t) + R^{-1}B^T r(t)$	7.0	8.3	14.3	8.3	7.0
$-Ky_c(t)$ (I)	3.3	7.7	11.2	7.7	3.3
$-Ky_c(t)$ (II)	4.7	7.5	10.7	7.5	4.7
$-Ky(t) + R^{-1}B^T r(t)$	7.1	8.3	14.3	8.3	7.0
$-Ky(t)$	4.7	7.5	10.7	7.5	4.7

Table 12c : *Example 4 - Cavity Excitation :* – Effects on the simulated rms velocity at 5 beam points for open loop, H^∞ full state controller with and without r(t) and for the H^∞ compensator with r(t) and Cases I, II. Results for the time interval $[\frac{3}{75}, \frac{30}{75}]$, with $\gamma^2 = 1$.

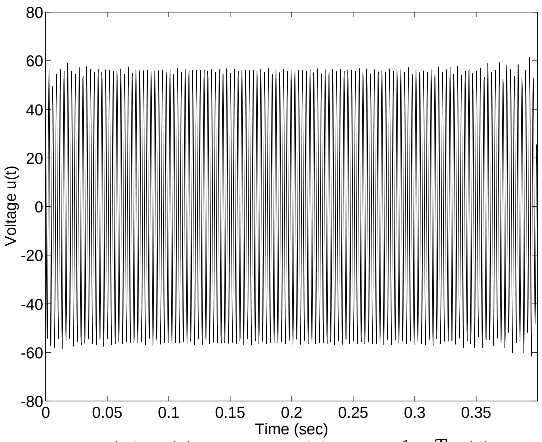

(a) $u(t) = -Ky_c(t) + R^{-1}B^T r(t)$

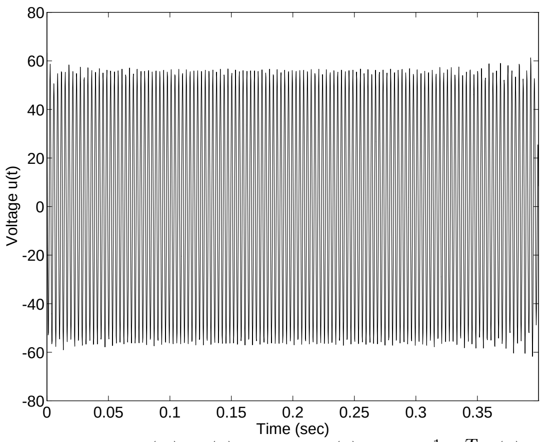

(d) $u(t) = -Ky(t) + R^{-1}B^T r(t)$

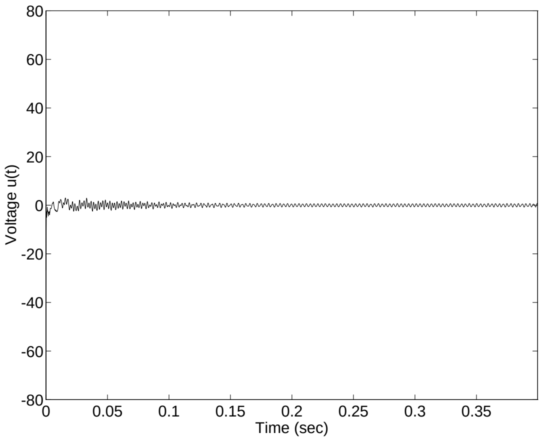

(b) $u(t) = -Ky_c(t)$ (I)

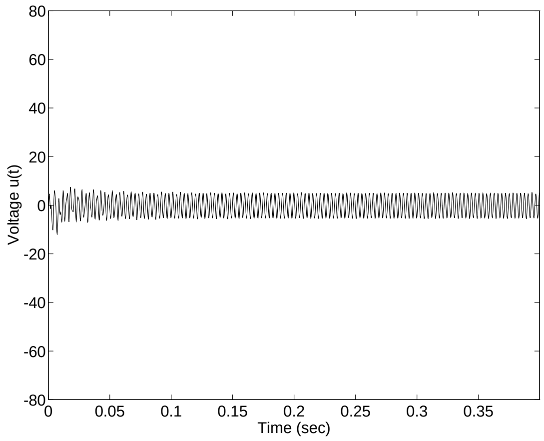

(e) $u(t) = -Ky(t)$

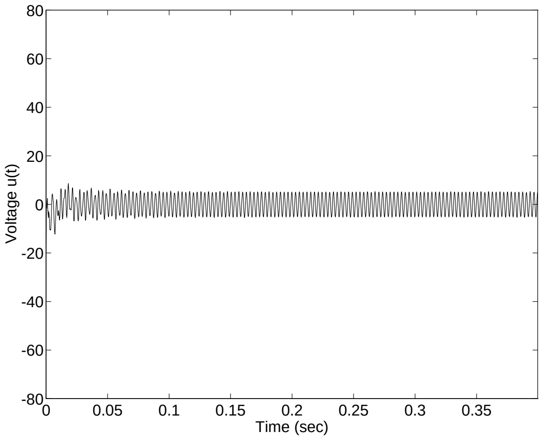

(c) $u(t) = -Ky_c(t)$ (II)

Figure 6: *Example 4 - Cavity Excitation :* Effects on the simulated voltage for H^∞ full state controller with and without $r(t)$ and for the H^∞ compensator with $r(t)$ and Cases I, II. Results for the time interval $[0, 0.4]$.

The above results indicate that the performance of Case I versus Case II is frequency-dependent. Both performances are between the open loop case and the full state controller with tracking signal included (the ideal case). No significant difference in performance is observed for the H^∞ compensator and full state controller with tracking signal included. In addition to the computational time saved when omitting the calculation for r, we also noted the reduced (rms) voltage for both cases (with the one for Case I somewhat less than that for Case II).

7 Conclusions

This report represents an extensive summary of our computational efforts on robustness and implementation issues concerning an H^∞-based compensator for structural acoustic models subjected to an exogenous driving force. Many difficulties arise when dealing with implementing controllers on large and complex systems, and we hope through this study to provide insights regarding computational and implementational issues encountered in applying H^∞ compensators to such systems.

Because of the persistent exogenous input, a modification to the standard compensator had to be made, namely the addition of a tracking signal which is a filtered version of the exogenous input. Due to the causal nature of the original system, this signal must first be integrated backward in time and then used in the control law. Some possibilities arise in excluding such a term from the controller. We found out that the compensator performance with the tracking signal excluded ranged between the open loop case and the case where this signal is included in the control law (ideal case). The results obtained with these options (on the exclusion of the tracking signal) appear to be frequency-dependent. Despite the fact that they are simpler to implement than the ideal case, a compromise must be made between their reduced performance and this implementational ease. Another positive aspect of these (tracking signal exclusion) options is the small size of the rms input voltage compared to the rms voltage for the ideal case. While disturbance attenuation of the above two (exclusion-of-the-tracking-signal) options is not as acceptable as in the ideal case, their reduced level of rms voltage makes them attractive from an energy point of view.

When implementing LQG and H^∞ compensators with tracking signal included, a number of issues affect the efficiency and performance. One factor that affects the stability properties of a controller, based on any methodology (H^∞, LQG, pole placement, adaptive, et cetera), is the introduction of time delays entering the input and output signals. Our studies suggest that for the structural acoustic system under consideration with control implemented in the manner described, delays in the input voltage result in unacceptable performance. Furthermore, the study suggests that small delays can be tolerated in the measured output without significantly affecting the overall performance and delays in the periodic forcing function leave the compensator performance almost unaltered.

Due to the nature of the exogenous signal (generated by exterior noise field), a correct measurement of exact frequency is generally not feasible; therefore some uncertainty in the frequency exists which manifests itself in a perturbation term that must be taken into account when designing the compensator. By ignoring such a term, where we essentially design the compensator based on its nominal component, we noted that more than a $\pm 1\%$ frequency error resulted in unacceptable performance. When the amplitude/frequency uncertainties were incorporated into the modeling uncertainties and were taken into account by the H^∞/MinMax control design, no improvement in the performance was observed.

The computations reported here suggest that for certain types of uncertainties neither the LQG/Kalman filter or the H^∞/MinMax control formulations provide adequate robustness. Specifically, several types of hardware induced delays which are inevitable in implementing these methods as well as frequency uncertainties in an exogenous disturbance are not handled with any real significant robustness in these formulations. This provides new challenges for control theorists who are interested in developing practical robust control methodologies. While "delay identification" techniques provide a partial solution to this problem in some cases, such techniques are difficult to implement in complex systems such as our structural acoustic system involving coupled components. In such systems, the successful implementation of feedback control methods may depend upon the development of new methods possessing adequate robustness with respect to exogenous frequency uncertainties, hardware-induced delays, and phase shifts in input and output signals.

References

[1] T. Başar and P. Bernhard, *H^∞-Optimal Control and Related Minimax Design Problems*, Birkhäuser, Boston-Basel-Berlin, 1991.

[2] H. T. Banks, D. E. Brown, V. L. Metcalf, R. J. Silcox, R. C. Smith, and Y. Wang, *A PDE-based methodology for modeling, parameter estimation, and feedback control in structural and structural acoustic systems*, CRSC Report 94-1, Center for Research in Scientific Computation, North Carolina State University, Raleigh, NC 27695-8205, January, 1994; in *Mathematics and Control in Smart Structures, SPIE*, pp. 311-320.

[3] H. T. Banks, M. A. Demetriou, and R. C. Smith, *Robust output feedback control in a 2-D structural acoustic model with piezoceramic actuators*, in Proceedings of the 1994 International Conference on Intelligent materials, Blacksburg, VA, C. A. Rogers, ed., Lancaster, PA, June, 5-8 1994, Technomics, Publ. Co., pp. 109–127.

[4] ——, *An H^∞/minmax periodic control in a 2-D structural acoustic model with piezoceramic actuators*, CRSC Report 94-9, Center for Research in Scientific Computation, North Carolina State University, Raleigh, NC 27695-8205, June, 1994; IEEE Trans. on Automatic Control, submitted.

[5] H. T. Banks, W. Fang, R. J. Silcox, and R. C. Smith, *Approximation methods for control of structural acoustics models with piezoceramic actuators*, Journal of Intelligent Material Systems and Structures, 4 (1993), pp. 98–116.

[6] H. T. Banks, K. Ito, and Y. Wang, *Well posedness for damped second order systems with unbounded input operators*, Differential and Integral Equations, (1995), pp. 587–606.

[7] H. T. Banks, S. Keeling, R. J. Silcox, and C. Wang, *Linear quadratic tracking problems in hilbert space: Application to optimal active noise suppression*, in Proc. 5th IFAC Symposium on Control of DPS, Perpignan, France, June 1989, pp. 191–193.

[8] H. T. Banks, R. J. Silcox, and R. C. Smith, *Numerical simulations of a coupled 3-d structural acoustics system*, in Proc. of the Second Conference on Recent Advances in Active Control of Sound and Vibration, Blacksburg, VA, 1993, pp. 85–97.

[9] ——, *The modeling and control of acoustic/structure interaction problems via piezoceramic actuators: 2-d numerical examples*, ASME Journal of Vibration and Acoustics, 116 (1994), pp. 386–396.

[10] H. T. Banks and R. C. Smith, *Modeling and approximation of a coupled 3-d structural acoustics problem*, in Computation and Control III: Proceedings of the Third Boseman Conference, K. Bowers and J. Lund, eds., Birkhäuser, Boston-Basel-Berlin, 1993, pp. 29–48.

[11] ——, *The modeling and approximation of a structural acoustics problem in a hard-walled cylindrical domain*, CRSC Report 94-26, Center for Research in Scientific Computation, North Carolina State University, Raleigh, NC 27695-8205, December 1994.

[12] ——, *Feedback control of noise in a 2-d nonlinear structural acoustics model*, Discrete and Continuous Dynamical Systems, 1 (1995), pp. 119–149.

[13] ——, *Models for control in smart material structures*, CRSC Report 92-21, Center for Research in Scientific Computation, North Carolina State University, Raleigh, NC 27695-8205, December, 1992; in *Identification and Control in Systems Governed by Partial Differential Equations*, SIAM, Philadelphia, 1993, pp. 26-44.

[14] ——, *Noise control in a 3-d structural acoustic system: numerical simulations*, CRSC Report 94-2, Center for Research in Scientific Computation, North Carolina State University, Raleigh, NC 27695-8205, February, 1994; in *Intelligent Materials*, (C. A. Rogers, ed.) Technomics Publ. Co., Lancaster, PA 1994, pp. 128-139.

[15] H. T. Banks, R. C. Smith, and Y. Wang, *Implementation issues regarding PDE-based controllers- control of transient and periodic plate vibrations*, preprint, (1995).

[16] ——, *Vibration suppression with approximate finite dimensional compensators for distributed parameter systems; computational methods and experimental results*, CRSC Report 94-3, Center for Research in Scientific Computation, North Carolina State University, Raleigh, NC 27695-8205, February, 1994; in *Intelligent Materials*, (C. A. Rogers, ed.) Technomics Publ. Co., Lancaster, PA 1994, pp. 140-154.

[17] ——, *Modeling aspects for piezoceramic patch activation of shells, plates and beams*, Tech. Report 92-12, Center for Research in Scientific Computation, North Carolina State University, Raleigh, NC 27695, November, 1992; Quarterly of Applied Mathematics, to appear.

[18] H. T. Banks, Y. Wang, D. J. Inman, and J. C. Slater, *Approximation and parameter identification for damped second order systems with unbounded input operators*, CRSC Report 93-9, Center for Research in Scientific Computation, North Carolina State University, Raleigh, NC 27695-8205, May, 1993; Control: Theory and Advanced Technology, 10 (1995), to appear.

[19] A. Bensoussan and P. Bernhard, *Remarks on the theory of robust control*, in Optimization, Optimal Control and Partial Differential Equations: First Franco-Romanian Conference, Iasi, V. Barbu, J. F. Bonnans, and D. Tiba, eds., vol. 107 of International

Series in Numerical Mathematics, Birkhäuser, Basel-Boston-Berlin, September 7-11 1992, pp. 149–166.

[20] T. Kailath, *Linear Systems*, Prentice-Hall, Inc., Englewood Cliffs, N.J., 1980.

[21] B. V. Keulen, *H_∞-Control for Distributed Parameter Systems: A State-Space Approach*, Birkhäuser, Boston-Basel-Berlin, 1993.

[22] ——, *The H_∞-problem with measurement feedback for linear infinite dimensional systems*, Journal of Mathematical Systems, Estimation, and Control, (to appear).

[23] D. J. N. Limebeer and Y. S. Hung, *An analysis of the pole-zero cancellations in H^∞-optimal control problems of the first kind*, SIAM J. Control and Optimization, 25 (1987), pp. 1457–1493.

[24] A. G. J. Macfarlane and N. Karcanias, *Poles and zeros of linear multivariable systems: a survey of the algebraic, geometric and complex-variable theory*, Int. J. Control, 24 (1976), pp. 33–74.

[25] H. H. Rosenbrock, *State-Space and Multivariable Theory*, John Wiley & Sons, Inc., New York, 1970.

[26] R. C. Smith, *A Galerkin Method for Linear PDE Systems in Circular Geometries with Structural Acoustic Applications*, Report 94-40, ICASE, 1994, *SIAM Journal of Scientific Computing*, submitted.

[27] A. Stoorvogel, *The H^∞ Control Problem*, Prentice Hall, Englewood Cliffs, NJ, 1992.

[28] K. Zhou, *Comparison between the $\mathcal{H}_2$ and $\mathcal{H}_\infty$ controllers*, IEEE Trans. on Automatic Control, 37 (1992), pp. 1261–1265.